In: Advances in Mechanical Engineering Research. Volume 2 ISBN: 978-1-61761-984-7
Editor: David E. Malach

Chapter 1

FRACTURE MECHANICS OF WOOD AND WOOD-LIKE REINFORCED POLYMERS

T.A.C.M. van der Put*

TU-Delft, Civil Engineering and Geosciences, Timber Structures and wood technology, PO Box 5048, NL-2600 GA Delft, Netherlands

ABSTRACT

This chapter discusses the theory of fracture mechanics based on the flat elliptical crack; the derivation of the mixed "mode I - II" - interaction equation, with the relations between the mode I and mode II stress intensities and energy release rates, based on an orthotropic-isotropic transformation of the Airy stress function; the derivation of the softening curve with the explanation of the measurements; the derivation of the power law; the energy method of notched beams and of joints loaded perpendicular to the grain; and the necessary rejection of the applied crack growth models and fictitious crack models.

1. INTRODUCTION

The development of the inexact singularity approach of fracture mechanics is at its dead end because it is not possible to describe real failure at the crack boundary and to replace the real failure criterion by general energy conditions as is applied now, and the method remains empirical. Therefore, the theoretical approach based on the elliptical flat crack has to be followed, leading to the possibility to derive and explain the empirical mixed "mode I - II" - interaction equation.

As a result of this derivation, the right fracture energy and theoretical relation between mode I and II stress intensities, and energy release rates are obtained. Based hereupon, the derivation of the orthotropic mode I strain softening curve is possible. It appears that real softening does not exist. It is a matter of unloading of the specimen outside the fracture zone

* Tel: +31 152851980, E-mail: vanderp@xs4all.nl

where the ultimate stress remains. This ultimate stress on the intact area of the fracture plane determines any moment the strength of every point of the softening curve. The area under the load-displacement softening curve gives the total external work on the test specimen and not the fracture energy. The fracture energy follows from half this area which is equal to the critical strain energy release rate at the initial crack extension. For wood, this correctly is applied for mode II. For mode I however, as for other materials, wrongly the total area is regarded as fracture energy, a factor 2 too high. However, this is compensated at softening by the apparent too low specific fracture energy due to a small crack joining mechanism when the ultimate state of the ligament of the test-specimen is reached. Post fracture behaviour thus is shown to be different from initial macro crack extension. The derivations lead to an adaption of the energy approach for fracture of square notched beams and joints loaded perpendicular to the grain,providing a simple design method. It further is shown that nearly all fracture mechanics models applied to wood, as the Dugdale model, the fictitious crack model and the crack growth models (which should follow from exact molecular deformation kinetics), are questionable and have to be replaced by the developed theory.

2. THE BOUNDARY VALUE PROBLEM OF FRACTURE MECHANICS

2.1. Basic Airy Stress Function

For the solution of the boundary value problem of notches in wood, the orthotropic Airy stress function is based on the spreading out of the reinforcement to act as a continuum, satisfying the equilibrium, compatibility and strength conditions. This behaviour only is possible by interaction of reinforcements through the matrix. Thus also the equilibrium conditions and strength criterion of the matrix, as determining element, have to be satisfied. This only is possible to solve the Airy stress function for the stresses in the isotropic matrix and then to derive the total (orthotropic) stresses from this solution. None of the applied solutions (given, e.g., in chapter 2.1 of [6]) satisfies this requirement. This analysis in total stresses is as follows:

The stress-strain relations for the two-dimensional flat crack problem are:

$$\varepsilon_x = c_{11}\sigma_x + c_{12}\sigma_y\,; \quad \varepsilon_y = c_{12}\sigma_x + c_{22}\sigma_y\,; \quad \gamma_{xy} = c_{66}\tau_{xy}\,. \tag{2.1}$$

This can be written:

$$\varepsilon_x = \sigma_x / E_x - \upsilon_{21}\sigma_y / E_y\,; \quad \varepsilon_y = -\nu_{21}\sigma_x / E_y + \sigma_y / E_y\,; \quad \gamma_{xy} = \tau_{xy} / G_{xy} \tag{2.2}$$

The Airy function follows from:

$$\sigma_x = \frac{\partial^2 U}{\partial y^2}\,; \quad \sigma_y = \frac{\partial^2 U}{\partial x^2}\,; \quad \tau_{xy} = -\frac{\partial^2 U}{\partial x \partial y}\,, \tag{2.3}$$

satisfying the equilibrium equations:

$$\frac{\partial \sigma_x}{\partial x}+\frac{\partial \tau}{\partial y}=0 \text{ and } \frac{\partial \tau}{\partial x}+\frac{\partial \sigma_y}{\partial y}=0 \tag{2.4}$$

Substitutions of eq.(2.1): $\varepsilon_x = c_{11}\frac{\partial^2 U}{\partial y^2}+c_{12}\frac{\partial^2 U}{\partial x^2}$, etc. in the compatibility condition:

$$\frac{\partial^2 \varepsilon_x}{\partial y^2}+\frac{\partial^2 \varepsilon_y}{\partial x^2}=\frac{\partial^2 \gamma_{xy}}{\partial x \partial y}, \tag{2.5}$$

gives:

$$c_{22}\frac{\partial^4 U}{\partial x^4}+\left(c_{66}+2c_{12}\right)\frac{\partial^4 U}{\partial x^2 \partial y^2}+c_{11}\frac{\partial^4 U}{\partial y^4}=0 \tag{2.6}$$

This equation also can given as:

$$\left(\frac{\partial^2}{\partial x^2}+\alpha_1\frac{\partial^2}{\partial y^2}\right)\left(\frac{\partial^2}{\partial x^2}+\alpha_2\frac{\partial^2}{\partial y^2}\right)U=0 \tag{2.7}$$

where $\alpha_1\alpha_2 = c_{11}/c_{22}$ and $\alpha_1+\alpha_2=\left(c_{66}+2c_{12}\right)/c_{22}$. Introducing 3 sets of polar coordinates for this case, $x+iy=re^{i\theta}$, $x+iy/\sqrt{\alpha_1}=re^{i\theta_1}$, $x+iy/\sqrt{\alpha_2}=re^{i\theta_2}$, eq.(2.7) has e.g. elementary solutions as: $r_1^{\pm m}\cos(m\theta_1)$, $r_1^{\pm m}\sin(m\theta_1)$, $r_2^{\pm m}\cos(m\theta_2)$, $r_2^{\pm m}\sin(m\theta_2)$, leading to:

$$\left\{\sigma_r,\sigma_\theta,\sigma_{r\theta}\right\}=\frac{K_A}{\left(2\pi r\right)^m}\left\{f_1(\theta),f_2(\theta),f_3(\theta)\right\} \tag{2.8}$$

in the vicinity of a notch root as stress singularity at $r = 0$,

As solution, always only smaller powers than $m = 0.5$ are found, showing the (isotropic) singularity approach with the power $m = 0.5$ to be not a real solution for an orthotropic material. Thus the singularity approach only may apply for the stresses of the isotropic wood-matrix. Wood acts as a reinforced material. Lignin is isotropic and hemicellulose and cellulose are transversely isotropic, which means that only one stiffness factor in the main direction has an n-fold higher stiffness in proportion to the higher stiffness of the reinforcement with respect to the matrix. Thus wood material can be treated to contain a shear-reinforcement and a tensile reinforcement in the main direction and eq.(2.9) applies for equilibrium of the matrix stresses:

$$\frac{\sigma_x}{n_1}=\frac{\partial^2 U}{\partial y^2};\quad \sigma_y=\frac{\partial^2 U}{\partial x^2};\quad \frac{\tau_{xy}}{n_6}=-\frac{\partial^2 U}{\partial x\partial y}, \tag{2.9}$$

Instead of using the matrix stresses and the matrix stiffness, the n-fold higher total stresses and n-fold higher stiffness can be used to give the same compatibility condition (thus the same condition for the matrix and reinforcement). Inserting the total stresses in the compatibility equation, eq.(2.5), gives:

$$c_{22}\frac{\partial^4 U}{\partial x^4}+\left(n_6 c_{66}+(1+n_1)c_{12}\right)\frac{\partial^4 U}{\partial x^2\partial y^2}+n_1 c_{11}\frac{\partial^4 U}{\partial y^4}=0 \tag{2.10}$$

For the isotropic matrix is: $n_1 c_{11}/c_{22}=1$ and $(n_6 c_{66}+(1+n_1)c_{12})/c_{22}=2$ giving:

$$\frac{\partial^4 U}{\partial x^4}+2\frac{\partial^4 U}{\partial x^2\partial y^2}+\frac{\partial^4 U}{\partial y^4}=\nabla^2(\nabla^2 U)=0 \tag{2.11}$$

and

$$n_1=\frac{c_{22}}{c_{11}}=\frac{E_x}{E_y};\quad n_6=\left(2-\frac{c_{12}}{c_{22}}-\frac{c_{12}}{c_{11}}\right)\cdot\frac{c_{22}}{c_{66}}=\left(2+\nu_{21}+\nu_{12}\right)\cdot\frac{G_{xy}}{E_y} \tag{2.12}$$

This orthotropic-isotropic transformation of the Airy stress function and the calculation method based on the matrix stresses is used in the following.

2.2. The Elliptical Flat Crack Solution

As shown above, the singularity approach does not apply for the orthotropic case andalso prevents the derivation of areal failure criterion. Instead of such a criterion, critical values are assumed of, e.g., the strain energy density, or the maximal principal stress, or a non local stress function, all at a distance away from the crack tip, thus away from the fracture site. A realfailure criterion only can be based on the real ultimate stress in the material which occurs near the crack-tip boundary. A real physical possible crack form is the flat elliptical crack. When “flow” occurs around the crack tip, the ultimate strain condition at the crack-boundary determines the extension of this flow area. The elastic-plastic boundary then acts as an enlarged crack boundary with the “flow”-stress as ultimate elastic stress for the linear elastic fracture mechanics calculation.

2.2.1. The Elliptic Hole in an Infinite Region

The classical way of analyzing the elliptic crack problem is to use complex variables and elliptic coordinates. The Airy stress function can be expressed in terms of two analytic

functions [1], of the complex variable z (= x + iy) and the transformation to elliptic coordinates in Figure 2.1, gives:

$z = x + iy = c \cdot \cosh(\xi + i\eta)$ or: $x = c \cdot \cosh(\xi) \cdot \cos(\eta)$; $y = c \cdot \sinh(\xi) \cdot \sin(\eta)$.

For an elliptic hole, $\xi = \xi_0$, in an infinite region with uniaxial stress *p* at infinity in a direction inclined at β to the major axis Ox of the ellipse, the Airy stress function *U*, satisfying $\nabla^2(\nabla^2 U) = 0$, and satisfying the conditions at infinity and at the surface $\xi = \xi_0$, showing no discontinuity of displacement, thus being the solution, is given in [2] and applied in [1]. Determining for the strengthis the tangential stress σ_t at the crack surface $\xi = \xi_0$ due to a stress *p* at an angle *β*(of Figure 2.3) to the crack

$$\sigma_t = \frac{p(\sinh(2\xi_0) + \cos(2\beta) - \exp(2\xi_0) \cdot \cos(2(\beta - \eta))}{\cosh(2\xi_0) - \cos(2\eta)} \tag{2.13}$$

eq.(2.13) can be extended for two mutual perpendicular principal stresses p_1 and p_2 (see Figure2.3) by a simple addition leading to eq.(2.23) below.

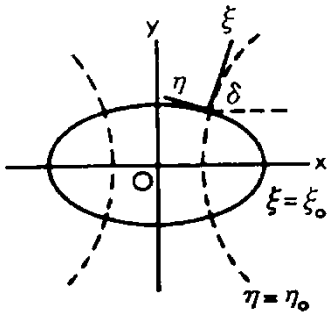

Figure 2.1 - Elliptic hole and coordinates.

2.2.2. The Mathematical Flat Crack Solution

For stresses in the wood-matrix, the results of the limit case of the elliptical notch with ξ_0 approaching zero should be comparable with the results of the mathematical flat crack of the singularity method. To obtain the singularity equations, new coordinates *X*, *Y* with the origin in the focus of the ellipse are necessary (see Figure 2.2). Thus:

$$X = x - c = c(\xi^2 - \eta^2)/2, \quad Y = y = c\xi\eta \tag{2.14}$$

or in polar coordinates:

$$r = \left(X^2 + Y^2\right)^{0.5}, \; X = r\cdot\cos(\theta), \; Y = r\cdot\sin(\theta) \tag{2.15}$$

and from eq.(2.14):

$$\xi^2+\eta^2=2\left(X^2+Y^2\right)^{0.5}/c=2r/c \tag{2.16}$$

$$\xi=\sqrt{2r/c}\cdot\cos\left(\theta/2\right),\quad \eta=\sqrt{2r/c}\cdot\sin\left(\theta/2\right),\quad \eta/\xi=\tan\left(\theta/2\right)=\tan\left(\delta\right) \tag{2.17}$$

To obtain the singularity, $\xi_0=0$ is inserted in the general solution of the elliptic Airy stress function, [1]. Then the tangential stress σ_θ along a crack boundary r_0, due to a stress p at infinity at an angle β with the notch is:

$$\left(8r_0/cp^2\right)^{0.5}\sigma_\theta=-3\sin\left(\theta/2\right)\cos^2\left(\theta/2\right)\sin\left(2\beta\right)+2\cos^3\left(\theta/2\right)\sin^2\left(\beta\right) \tag{2.18}$$

for a small value of r_0, so that all terms containing not the factor $r_0^{-0.5}$ are negligible. For the, for wood always applied, singularity method, the flat crack in the grain direction is supposed to propagate in that direction. Thus θ = 0 and eq.(2.18) becomes:

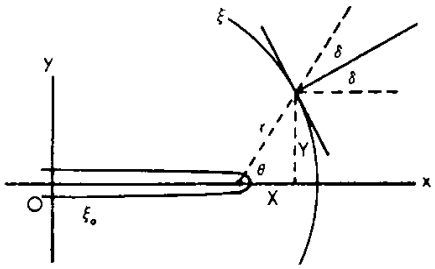

Figure 2.2. Confocal coordinates.

$$\left(8r/cp^2\right)^{0.5}\sigma_\theta=2\sin^2\left(\beta\right) \tag{2.19}$$

with $\sigma_r=\sigma_\theta$ and $\tau_{r\theta}=\sigma_\theta$ cotg(β). Mode I failure $\sigma_\theta=\sigma_t$ occurs when $\beta=\pi/2$. Thus when:

$$p=\sigma_t\sqrt{(2r_0/c)} \tag{2.20}$$

For pure shear loading, thus for superposition of $p_1=S$ at β = π/4 and $p_2=-S$ at β = 3π/4 in eq.(18) and in the other equations of the solution is for crack extensionθ = 0:

$$\left(2r/cS^2\right)^{0.5}\tau_{r\theta}=\left(\cos(\theta/2)\cdot\left(3\cos^2(\theta/2)-2\right)\right)_{\theta=0}=1$$

or :

$$S=\tau_{r\theta}\sqrt{(2r_0/c)} \tag{2.21}$$

with now $\sigma_r=\sigma_\theta=0$, leading to an ultimate shear failure criterion.

Eq.(2.20) and (2.21) are maximum stress conditions for the strengths in the main planes. Thus fracture is predicted to occur when the tensile strength is reached perpendicular to the grain and/or when the shear strength in this plane is reached. Thus: $K_I \le K_{Ic}$ and $K_{II} \le K_{IIc}$ for all stress states (without the interaction). This also is predicted for the n-fold higher orthotropic stresses and is shown by eq.(2.30) to be not right.Thus also for the isotropic matrix, the applied singularity approach gives no right results. The right failure condition for combined stresses is derived below. The singularity failure equations are applicable as lower bound solution for matrix stresses by a chosen equilibrium system for co-axial macro-crack propagation as applied below for fracture of joints and beams with square end-notches, wherefore the mode I energy release rate is chosen as specific fracture energy.

2.3. Derivation of the Mixed I- II- Mode Equation

A general failure criterion [3] follows from the limited ultimate tensile stress which occurs at the crack boundary. By an extension of eq.(2.13) (by superposition) to $p_1=\sigma_1$ inclined at an angle $\pi/2 + \beta$ to the Ox-axis and $p_2=\sigma_2$ inclined at an angle β, (see Figure2.3), eq.(2.13) turns to:

$$\sigma_t=\frac{2\sigma_y\sinh(2\xi_0)+2\tau_{xy}[(1+\sinh(2\xi_0))\cdot\cot(2\beta)-\exp(2\xi_0)\cdot\cos(2(\beta-\eta))\,\mathrm{cosec}(2\beta)]}{\cosh(2\xi_0)-\cos(2\eta)}, \tag{2.22}$$

where the stresses are given in notch coordinates with the x-axis along the notch. For small values of ξ_0 and η (flat notches), this equation becomes:

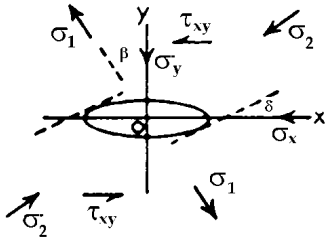

Figure 2.3. Stresses in the notch plane Ox.

$$\sigma_t = \frac{2\left(\xi_0\sigma_y - \eta\tau_{xy}\right)}{\xi_0^2 + \eta^2} \tag{2.23}$$

The maximum (critical) value of the tangential tensile stress σ_t, depending on location η, is found by: $d\sigma_t / d\eta = 0$, giving the critical value of η:

$$-2\tau_{xy} / \left(\xi_0^2 + \eta^2\right) - \left(2\left(\xi_0\sigma_y - \eta\tau_{xy}\right)\cdot 2\eta\right) / \left(\xi_0^2 + \eta^2\right)^2 = 0,$$

or:

$$-\tau_{xy}\left(\xi_0^2 + \eta^2\right) = 2\eta\left(\xi_0\sigma_y - \eta\tau_{xy}\right) = \eta\sigma_t\left(\xi_0^2 + \eta^2\right) \tag{2.24}$$

where the second equality sign is due to the substitution of eq.(2.23).
From the first and last term follows that:

$$\eta\sigma_t = -\tau_{xy} \tag{2.25}$$

and from the first 2 terms:

$$\eta / \xi_0 = \left(\sigma_y \pm \sqrt{\sigma_y^2 + \tau_{xy}^2}\right) / \tau_{xy} \tag{2.26}$$

or with eq.(2.23):

$$\xi_0\sigma_t = \sigma_y \pm \sqrt{\sigma_y^2 + \tau_{xy}^2} \tag{2.27}$$

and eq.(2.27) can be written:

$$1 = \frac{\sigma_y}{\xi_0\sigma_t / 2} + \frac{\tau_{xy}^2}{\xi_0^2\sigma_t^2} \tag{2.28}$$

According to eq.(2.17) is, for small values of θ at the crack tip: $\xi_0 = \sqrt{2r_0 / c}$, giving in eq.(2.28):

$$1 = \frac{\sigma_y\sqrt{\pi c}}{\sigma_t\sqrt{2\pi r_0} / 2} + \frac{\left(\tau_{xy}\sqrt{\pi c}\right)^2}{\left(\sigma_t\sqrt{2\pi r_0}\right)^2} \tag{2.29}$$

which is identical to the empirical parabolic interaction equation of Wu [4], measured on Balsa and on fiber reinforced plastic plates:

$$\frac{K_I}{K_{Ic}} + \frac{\left(K_{II}\right)^2}{\left(K_{IIc}\right)^2} = 1 \tag{2.30}$$

The fact that $K_{IC} = \sigma_y \sqrt{\pi c_c} = \sigma_t \sqrt{\pi r_0 / 2}$ is constant and therefore is regarded as material property, shows that failure is always by the same initial small cracks with tip-radius r_0 by the uniaxial cohesion strength σ_t. This applies for every level down to the molecular level. In [7] the estimation method of the relation between engineering macro stresses and molecular stresses at the bond breaking sites is given. For Balsa wood with a low density of reinforcement, nearly isotropic strength behaviour is found for crack extension. Thus $K_{IIc} = 2K_{Ic}$ according to eq.(2.28) and (2.30) as verified by the data of Wu of Balsa by: $K_{IIc} \approx 140\,\mathrm{psi}\cdot\mathrm{in}^{0.5}$ and $K_{Ic} \approx 60\,\mathrm{psi}\cdot\mathrm{in}^{0.5}$.

Eq.(2.30) is generally applicable also when σ_y is a compression stress as follows from the measurements of Figure 2.4. When the compression is high enough to close the small notches ($\sigma_{y,cl} \approx 2G_{xy}\xi_0$), τ_{xy} has to be replaced by the effective shear stress: $\tau^*_{xy} = \tau_{xy} + \mu\left(\sigma_y - \sigma_{y,cl}\right)$ in eq.(2.28) or:

$$1 = \frac{\sigma_{y,cl}}{\xi_0 \sigma_t / 2} + \frac{\left(\tau^*_{xy}\right)^2}{\xi_0^2 \sigma_t^2}, \tag{2.31}$$

what is fully able to explain fracture by compression perpendicular to the notch plane (see Figure 2.4). In this equation is μ the friction coefficient.

For species, with denser layers than those of Balsa, a much higher value of K_{IIc} than twice the value of K_{Ic} is measured because due to the reinforcement, η is smaller than the isotropic critical value of eq.(2.26). To read the equation in applied total orthotropic stress values, the matrix stress τ_{iso} has to be replaced by τ_{ort} / n_6 and the maximum slope of the tangent, slope δ in Figure 2.2 of the location of the failure stress, is:

$$\left|\tan\delta\right| = \left|\eta_m\right| / \xi_0 = K_{Ic} / K_{IIc} = 1 / 2n_6 \tag{2.32}$$

For small values of $\eta = -|\eta|$, eq.(2.23) can be written, neglecting $(\eta/\xi_0)^2$:

$$\frac{\sigma_y}{\xi_0\sigma_t/2}=1+\frac{\eta^2}{\xi^2}-\frac{\tau_{xy}}{\xi_0^2\sigma_t/\left(2|\eta|\right)}\approx 1-\frac{\tau_{xy}}{\xi_0^2\sigma_t/\left(2|\eta|\right)} \tag{2.33}$$

where $|\eta|$ is the absolute value of negative η. Thus:

$$\frac{K_I}{K_{Ic}}+\frac{K_{II}}{K_{IIc}}\approx 1 \tag{2.34}$$

This is a lower bound, with:

$$K_{IIc}=\left(\xi_0/|\eta_m|\right)\cdot K_{Ic} \tag{2.35}$$

and the maximal value of $\eta=\eta_m$ is found by measuring K_{Ic} and K_{IIc}, giving e.g. a value of about $\xi_0/\eta_m\approx 7.7$, showing that the disregard of $\left(\eta/\xi_0\right)^2$ = 0.017 with respect to 1 is right. Measurements between the lines eq.(2.30) and (2.34) thus indicate a strong difference between K_{IIc} and K_{Ic} of the local structure that is crossed by the propagating crack.

Thus far, the equations are given in matrix stresses. To change this in the real applied orthotropic stresses, $\tau_{iso}=\tau_{ort}/n_6$ has to be inserted in eq.(2.28) giving:

$$1=\frac{\sigma_y}{\xi_0\sigma_t/2}+\frac{\tau_{iso}^2}{\xi_0^2\sigma_t^2}=\frac{\sigma_y}{\xi_0\sigma_t/2}+\frac{\tau_{ort}^2}{\xi_0^2\sigma_t^2n_6^2}=\frac{K_I}{K_{Ic}}+\frac{\left(K_{II}\right)^2}{\left(K_{IIc}\right)^2} \tag{2.36}$$

and it follows that:

$$\frac{K_{IIc}}{K_{Ic}}=\frac{\xi_0\sigma_t n_6}{\xi_0\sigma_t/2}=2n_6 \tag{2.37}$$

according to eq.(2.12) is e.g. for small clear specimens:

$2n_6=2\cdot\left(2+\nu_{21}+\nu_{12}\right)\cdot\left(G_{xy}/E_y\right)$ = 2(2 + 0.57)/0.67 = 7.7 for Spruce

and: 2(2 + 0.48)/0.64 = 7.7 for Douglas Fir in TL-direction.

This is in this case independent of the densities of respectively 0.37 and 0.50 at a moisture content of 12 %. Thus, for $K_{Ic}\approx 265\,kN/m^{1.5}$ is

$K_{IIc} = 7.7 \cdot 265 = 2041\ kN/m^{1.5}$ in the TL-direction. This agrees with measurements [6]. In RL-direction this factor is 3.3 to 4.4. Thus, when K_{IIc} is the same as in the TL-direction, the strength in RL-direction is predicted to be a factor 1.7 to 2.3 higher with respect to the TL-direction. This however applies at high crack velocities ("elastic" failure) and is also dependent on the site of the notch. At common loading rates a factor lower than 410/260 = 1.6 is measured [6] and at lower cracking speeds, this strength factor is expected to be about 1 when fracture is in the "isotropic" middle lamella. It then thus is independent of the TL and RL-direction according to the local stiffness and rigidity values. To know the mean influence, it is necessary to analyze fracture strength data dependent on the density and the elastic constants of n_6. From the rate dependency of the strength follows an influence of viscous and viscoelastic processes. This has to be analyzed by Deformation Kinetics [7].

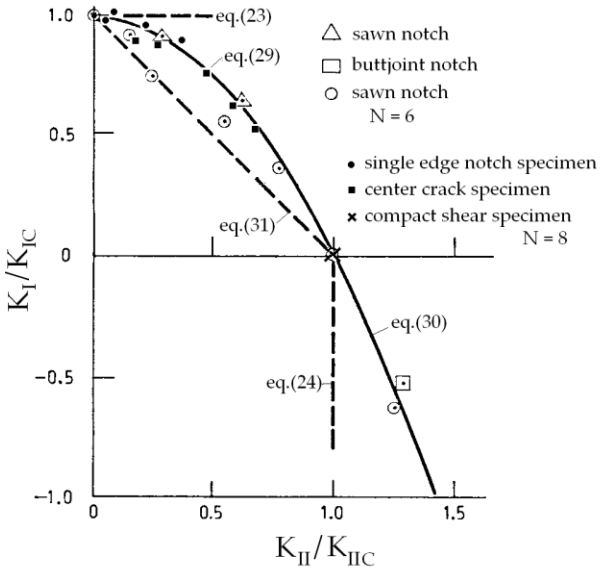

Figure 2.4. Fracture strength under combined stresses [5], [6].

A general problem is further the possible early instability of the mode I-tests. This means thatsmall-cracks failure outside the notch-tip region may be determining as e.g. in the tests of [6]. In thiscase constants should be compared with the related to mode II data.

2.4. Remarks Regarding Crack Propagation

Because the mixed mode failure criterion shows that crackstends to propagates in the direction perpendicular to greatest principal tensile stress, the, in literature mentioned, empirical principle, that the crack follows the direction that maximises G, the energy release, is now explained to be the result of the failure criterion. This maximizing G principle does not hold and is opposite principle a compression stress. Then the crack direction tends to become parallel to the stress where the crack is not any more affected by this stress. For wood these maximizing and minimizing principles don't apply, because fracture follows the weak planes

along the grain and jumps periodically to the next growth layer in a zigzag way around the critical direction, determined by the Wu failure criterion

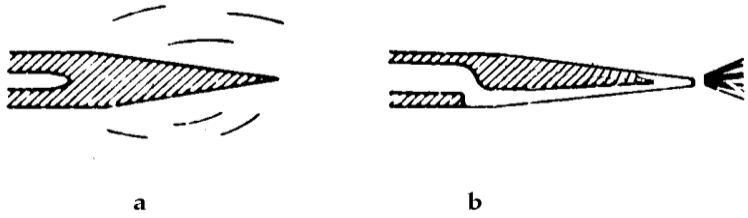

Figure2.5. a) Crazing at the crack tip and b) Possible crack extension along the fractured zone in glassy polymers.

In Figure2.5-b, it can be seen that mixed mode crack propagation starts at an angle with its plane but may bend back along the fractured zone to its original direction where crazing and fractured zone formation starts again. Stage b of this crack propagation is due to small-cracks merging from the fractured zone which extend to the macro-crack tip. For wood stage b occurs in a parallel crack plane. Co-axial crack propagation in this case is due to the small-crack joining mechanism discussed below. If, by the high stress near the macro-crack tip, each two adjacent small cracks in the weak main plane propagate towards each other, their out of plane directions for crack extension are opposed causing tensile stress interference in this weak plane which is sufficient for crack propagation in this plane because of the sufficiently close mutual distances in the critical state.

2.5. Additional Remarks Regarding the Empirical Confirmation

Measurements are given in Figure2.4. The points are mean values of a series of 6 or 8 specimens. The theoretical line eq.(2.30) is also the mean value of the extended measurements of Wu on balsa plates. Only the Australian sawn notch data deviate from this parabolic line and lie between eq.(2.30) and the theoretical lower bound eq.(2.34). This is explained by the theory of a too high K_{IIc}/K_{Ic}-ratio, indicating a mistake in manufacture. The theoretical prediction that $K_{IIc} = 2K_{Ic}$, for dominant isotropic behaviour of the matrix, is verified for Balsa with its very low fiber density. The prediction that $K_{IIc}/K_{Ic} = 2\cdot(2+\nu_{21}+\nu_{12})\cdot(G_{xy}/E_y)$ agrees with the measurements, using general mean values of the constants. However, precise, local values of the constants at the notches are not measurable and there is an influence of the loading rate and cracking speed. Thus safe lower bound values have to be used in practice.

The theory also fully explains the influence of compression perpendicular to the notch plane on the shear strength, eq.(2.31) in Figure 2.4.

The conclusion thus is that all measurements are explained by the theory.

2.6. References

[1] van der Put T.A.C.M., A new fracture mechanics theory for orthotropic materials like wood, *Engin. Fract. Mech*. 74, (2007) 771-781.
[2] Timoshenko S. and Goodier J.N., *Theory of elasticity*, McGraw-Hill bookcomp., N.Y. 1951, 179-204.
[3] van der Put, T.A.C.M., Explanation of the mixed mode interaction equation, COST 508 workshop 2, Bordeaux, April 1992
[4] Wu E.M., Application of fracture mechanics to anisotropic plates, *ASME J. Appl. Mech*. *Series E*, 34 4, Dec. 1967, pp. 967-974..
[5] Leicester R.H., Fracture strength of wood, First Australian Conf. on Engin. Materials, Univ. of New South Wales, 1974.
[6] RILEM state of the art report on fracture mechanics, Espoo, 1991.
[7] van der Put, T.A.C.M., *Deformation and damage processes in wood*, Delft University press, 1989.

3. MODE I SOFTENING BEHAVIOUR AND FRACTURE ENERGY

3.1. Introduction

The derivation of the softening behaviour is discussed and it is shown that the area under the load-displacement softening curve of, e.g.,Figure3.3, 3.4, 3.6 or 3.7, divided by the crack area,is not the fracture energy, but the total external work of the fracture process. The fracture energy ishalf this valueand is equal to the critical strain energy release rate at the top of the curve. For wood this correctlyis applied for mode II. For mode I a two times too high value is applied as done for other materials. The fracture energy is a function of the Griffith strength and, as the strain energy release rate, related to the effective width of the test specimen and not to the length of the fracture plane. The strain energy release rate is determined at the top of the top of the softening curve as start of macro-crack extension. This top is determined by the critical small-crack density. Proceeded small-crack extension also determines the softening curve and post fracture behaviour.

The analysis is based on matrix stresses for mode I failure in the weak planes because of the necessary correction of the fracture energy. The analysis, according to the equilibrium method, then is the same as for an isotropic material.

Authors of fracture mechanics of wood call the plane of co-axial crack propagation, in the test specimen, the ligament, probably because a crack may extend over a part of the width of the specimen, causing the formation of a ligament which has to collapse, for a total crack extension. Because of possible misunderstanding this plane is further called “fracture plain”.

3.2. Compliance and Energy Release Rate

As most materials, wood shows near failure an apparent plastic behaviour and the loading curve can be approximated by equivalent elastic-plastic behaviour. Therefore linear elastic

fracture mechanics can be applied based on the ultimate stress at the elastic-plastic boundary around the crack tip. The dissipation by microcracking, plastic deformation and friction within this boundary, called fracture process zone, then is regarded as part of the fracture energy of the macro crack extension. Also the equilibrium method is applicable. When a specimen is loaded until just before the start of softening and then unloaded and reloaded, the behaviour is elastic until failure making the linear elastic derivation of the softening curve possible based on the derivation of the compliance of the fractured specimen as follows:

In Figure 3.1, a mode I, center notched test specimen is given with a length "*l*", a width "*b*" and thickness "*t*", loaded by a stress σ showing a displacement δ of the loaded boundary due to a small crack extension. The work done by the constant external stress σ on this specimen, during this crack extension is equal to

$$\sigma \cdot b \cdot t \cdot \delta = 2W \tag{3.1}$$

This is twice the increase of the strain energy *W* of the specimen. Thus the other half of the external work, equal to the amount *W*, is the fracture energy, used for crack extension. Thus the fracture energy is equal to half the applied external energy which is equal to the strain energy increase *W* and follows, for the total crack length, from the difference of the strain energy of a body containing the crack and of the same body without a crack:

$$\frac{\sigma^2}{2E_{eff}} blt - \frac{\sigma^2}{2E} blt = W \tag{3.2}$$

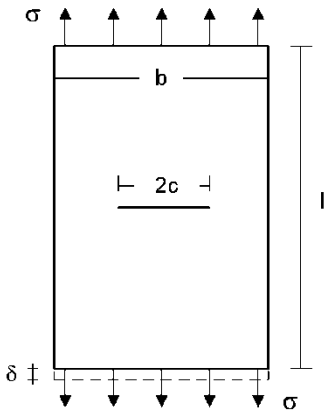

Figure 3.1. Specimen *b* x *l* and thickness *t*, containing a flat crack of 2*c*.

The fracture energy is also equal to the strain energy decrease at fixed grips conditions when $\delta = 0$:

$$W = t\sigma \int_{-c}^{+c} v da \; = \; \pi \sigma^2 c^2 t / E \tag{3.3}$$

where the last two terms give the strain energy to open (or to close) the flat elliptical crack of length 2*c* and where "*v*" is the displacement of the crack surface in the direction of σ. From eq.(3.2) and eq.(3.3) follows that:

$$\frac{\sigma^2}{2E_{eff}} blt - \frac{\sigma^2}{2E} blt = \pi\sigma^2 c^2 t / E \tag{3.4}$$

Thus the effective Young's modulus of the specimen of Figure 3.1, containing a crack of 2*c*, is:

$$E_{eff} = \frac{E}{1 + 2\pi c^2 / bl} \tag{3.5}$$

The equilibrium condition of the critical crack length is:

$$\frac{\partial}{\partial c}\left(W - G_c 2ct\right) = 0 \tag{3.6}$$

where G_c is the fracture energy for the formation of the crack surface per unit crack area. Eq.(3.6) also can be regarded as the law of energy conservation of Thermodynamics. Because $G_c = \partial W/\partial(2ct)$, it clearly also is a strain energy release rate when applied to eq.(3.3).

With *W* of eq.(3.2) or of eq.(3.3), eq.(3.6) becomes:

$$\frac{\partial}{\partial c}\left[\frac{\pi\sigma^2 c^2 t}{E} - G_c 2ct\right] = 0,$$

or:

$$\frac{\partial}{\partial c}\left[\frac{\sigma^2 blt}{2E}\left(1 + \frac{2\pi c^2}{bl}\right) - \frac{\sigma^2 blt}{2E} - G_c 2ct\right] = 0 \tag{3.7}$$

giving both the Griffith strength:

$$\sigma_g = \sqrt{\frac{G_c E}{\pi c}} \tag{3.8}$$

This stress is related to the width *b* of the specimen of Figure 3.1. The real mean stress in the determining weakest cross section with width $b - 2c$, where fracture occurs, is:

$$\sigma_r = \sqrt{\frac{G_c E}{\pi c}} \cdot \frac{b}{b-2c} = \sqrt{\frac{G_c E}{\pi b}} \cdot \frac{1}{(\sqrt{c/b}) \cdot (1-2c/b)} \tag{3.9}$$

and:

$$\frac{\partial \sigma_r}{\partial(\sqrt{c/b})} = \sqrt{\frac{G_c E}{\pi b}} \cdot \frac{6c/b-1}{(c/b) \cdot (1-2c/b)^2} > 0\,, \tag{3.10}$$

when *c/b*> 1/6, what always is the case for critical crack lengths. Thus the real stress σ_r increases monotonically with the increase of the crack length *c* and no softening behaviour exists at the critical site. Softening thus only exists outside the critical cross section and is identical to elastic unloading of the specimen outside the fracture zone in order to maintain equilibrium. Softening thus is not a material property as is assumed in the existing models for wood and other materials.

3.3. The Softening Curve

Softening should be described by the damage theory of Deformation Kinetics [1] but a simple description of the softening behaviour as a result of former crack propagation alone is possible by the Griffith theory. Straining the specimen of Figure 3.1 to the ultimate load at which the initial crack will grow, gives, according to eq.(3.5):

$$\varepsilon_g = \sigma_g / E_{eff} = \sigma_g \cdot (1 + 2\pi c^2 / bl) / E \tag{3.11}$$

Substitution of $c = G_c E / \pi \sigma_g^2$, according to eq.(3.8), gives:

$$\varepsilon_g = \sigma_g / E + 2G_c^2 E / \pi \sigma_g^3 bl \tag{3.12}$$

This is the equation of critical equilibrium states applying along the softening curve (for a not limiting, sufficient long length of the fracture plane of the test specimen). This curve, called Griffith locus, has a vertical tangent $d\varepsilon_g / d\sigma_g = 0$, occurring at a crack length of:

$$c_c = \sqrt{bl/6\pi}\,. \tag{3.13}$$

Smaller cracks than $2c_c$ are unstable because of the positive slope of the locus (according to eq.(3.16)). These small cracks, (near the macro-crack tip) extend during the loading stage, by the high peak stresses at the notch of the test specimen, to a stable length and only higher crack lengths than $2c_c$ are to be expected at the highest stress before softening, giving the stress-strain curve of Figure3.2 with σ_c as top value.

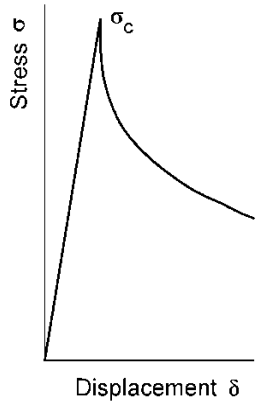

Figure3.2. Softening curve according to eq.(3.12) for the specimen of Figure3.1 or 3.5.

For a distribution of small cracks, *b* and *l* in eq.(3.13) are the crack distances and the critical crack distance for extension is about 2.2 times the crack length.Because, when $b \approx 2.2\cdot(2c_c)$ and $l \approx 2.2\cdot(2c_c)$, then$bl \approx 19\cdot c_c^2 \approx 6\pi c_c^2$ according to eq.(3.13). This critical distance also is predicted by Deformation Kinetics [1] and is used in Section3.6 to explain softening by small-crack propagation in the fracture plane.

According to eq.(3.13), the softening line eq.(3.12) now can be given as:

$$\varepsilon_g = \frac{\sigma_g}{E}\left(1+\frac{\sigma_c^4}{3\sigma_g^4}\right), \tag{3.14}$$

where

$$\sigma_c = \sqrt{EG_c/\pi c_c} \tag{3.15}$$

is the ultimate load with c_c according to eq.(3.13). The negative slope of the stable part of the Griffith locus, being the softening line, is:

$$\frac{\partial\sigma_g}{\partial\varepsilon_g} = -\frac{E}{\frac{\sigma_c^4}{\sigma_g^4}-1} = -\frac{E}{\frac{c^2}{c_c^2}-1} \tag{3.16}$$

Vertical yield drop occurs at the top at $\sigma_g = \sigma_c$, and the strain then is: $\varepsilon_{gc} = (\sigma_c/E)\cdot(1+1/3)$ and eq.(3.14) becomes:

$$\frac{\varepsilon_g}{\varepsilon_{gc}} = 0.75 \cdot \left(\frac{\sigma_g}{\sigma_c} + \frac{\sigma_c^3}{3\sigma_g^3} \right), \tag{3.17}$$

More in general eq.(3.14) can be written, when related to a chosen stress level σ_{g1}:

$$\frac{\varepsilon_g}{\varepsilon_{g1}} = \frac{\sigma_g}{\sigma_{g1}} \cdot \frac{1+\sigma_c^4/3\sigma_g^4}{1+\sigma_c^4/3\sigma_{g1}^4} \tag{3.18}$$

To control whether σ_c changes, eq.(3.18) can be written like:

$$\frac{\sigma_c}{\sigma_{g1}} = \left(\frac{3 \cdot (\sigma_g/\sigma_{g1})^3 \cdot \left((\varepsilon_g/\varepsilon_{g1}) - (\sigma_g/\sigma_{g1}) \right)}{1-(\varepsilon_g/\varepsilon_{g1}) \cdot (\sigma_g/\sigma_{g1})^3} \right)^{0.25} \tag{3.19}$$

with the measured values at the right hand side of the equation. When the occurring softening curve starts to differ from the Griffith locus, σ_c decreases, causing a steeper decline of the curve, due to additional clear wood failure of the fracture plane. This small-crack joining mechanism is discussed in Section 3.6.

3.4. Fracture Energy as Area Under the Softening Curve

The basic theory of the energy method, leading to eq.(3.1) and (3.2), should be confirmed by the loading curve (Figure3.3 and 3.4). This will be discussed in the now following.

When a test specimen is mechanical conditioned, the effective stiffness is obtained given e.g. by the lines OA and OC in Figure 3.3 and 3.4. In Figure3.3, the area OAB, written as A_{OAB}, is the strain energy of the specimen of Figure3.1 with a central crack (or with two side cracksaccording to Figure3.5) with a width "*b*", length "*l*" and thickness "*t*", loaded to the stress σ.

During the quasi static crack extension from B to D in Figure3.3, the constant external load σ does the work on the specimen of: $\sigma \cdot b \cdot t \cdot \Delta\varepsilon_{BD} \cdot l = \sigma \cdot b \cdot t \cdot \delta_{BD} = A_{ABDC}$, where $\Delta\varepsilon_{BD}$ is the strain increase due to the cracking and δ_{BD} the corresponding displacement. The strain energy after the crack extension is A_{OCD} and the strain energy increase by the crack extension thus is in Figure3.3: A_{OCD} - A_{OAB} = A_{OCD} - A_{OCB} = A_{CBD} = $A_{ABDC}/2$,

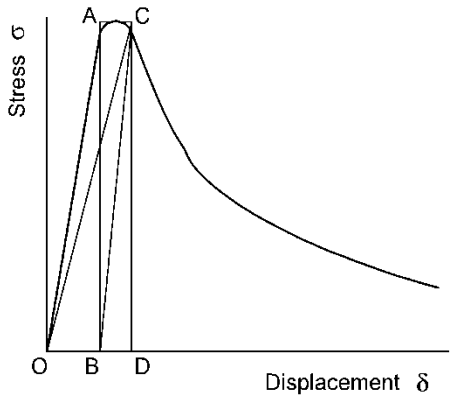

Figure3.3. Stress - displacement curve for tension, of the specimen of Figure3.1 or 3.5.

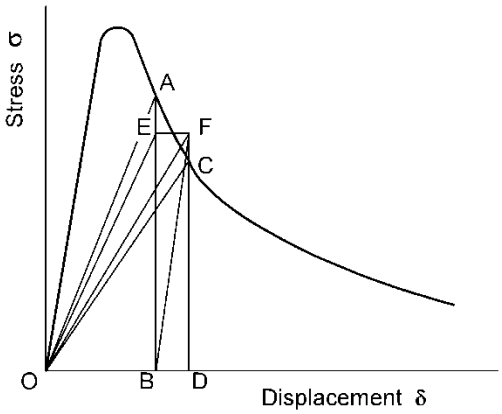

Figure3.4. Descending branch of the stress - displacement curve of Figure3.3.

Thus half of the external energy: $A_{ABDC} = \sigma \cdot b \cdot t \cdot \delta_{BD} / 2$ is the amount of increase of the strain energy due to the elongation by δ, and the other half thus is the fracture energy which is equal to this increase of strain energy.The same follows at unloading at yield drop. Because every point of the softening curve gives the Griffith strength, which decreases with increasing crack length, unloading is necessary to maintain equilibrium. The fracture with unloading step AC in Figure 3.4 is energetic equivalent to the unloading steps AE and FC and the fracturing step EF at constant stress EB = FD = (AB +DC)/2. Thus $A_{ABDC} = A_{EBDF}$. Identical to the first case of Figure3.3, the increase in strain energy due to crack extension is:

$$A_{ODF} - A_{OBE} = A_{ODF} - A_{OBF} = A_{BFD} = 0.5 \cdot A_{EBDF} = 0.5 \cdot A_{ABDC},$$

equal to half the work done by the external stresses during crack propagation and thus also equal to the other half, the work of crack extension. It thus is shown that half the area under the load-displacement curve represents the fracture energy. For mode II, only line OACO in

Figure3.3 is measured and A_{OAC} is regarded to be the fracture energy. Because $A_{OAC} = A_{BAC} = 0.5 \cdot A_{ABDC}$, thus equal to half the area under the load displacement curve, the right value is measured and mode II needs no correction.

Because eq.(3.2) is based on the total crack length and the strength is a Griffith stress, the initial value 2*c* of the crack length should be accounted and σ and G_c should be related to the whole crack length, including the initial value, and thus should be related to the whole specimen width *b* and not to the reduced width of the fracture plane: *b* – 2*c* as is done now. After the correction by a factor 2, this is the second necessary correction of the mode I fracture energy G_c. A third correction occurs when σ_c of eq.(3.14) changes. The apparent decrease of G_c at the end stage of the fracture process is due to an additional reduction of the intact area of the fracture plane of the specimen due to an additional clear-wood failure mechanism discussed in Section 3.6.

In [2], not $A_{ABDC}/2$ is regarded for the fracture energy the totally different amount A_{OACO} of Fig 3.3. This is the irreversible energy of a loading cycle by a crack increment when the specimen is regarded as one giant molecule. The elastic unloading-energies outside the fracture plane of: A_{OEA} and A_{OCF} are now additional measures of the bond reduction for the total specimen, representing a decrease of the apparent enthalpy and entropy terms of the activation energy. The triangle A_{OACO} thus represents the activation energy of the process [1] which is equal to the reversible work done on the system also represented by A_{OACO}. This is the case because this elastic energy is given by the elastic unloading parts, outside the fracture plane A_{OEA} and A_{OCF} together with A_{OEF}, the strain energy increase. As discussed in [3], the measurements of [2] indicate the presence of a mechanosorptive process, acting in the whole specimen. Thus A_{OACO} gives no separate information on the fracture process at the fracture plane and should not be applied as measure of the fracture energy.

3.5. Empirical Confirmation

The measurements of [4] are complete by measuring the whole loading and softening curve and using the compact tension tests as control, being a control by the different loading case.

The graphs of [4], Figure3.6 and 3.7, are the result of tension tests on the specimen of Figure 3.5.

The length of the specimen was *l* = 3 mm, the width and thickness: *b* = *t* = 20 mm and the notch length 2*c* = 2x5 = 10 mm with a notch width of 0.5 mm.

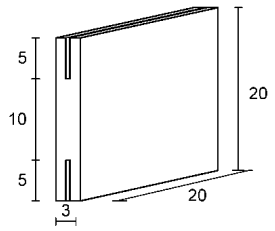

Figure3.5. Geometry of the specimens [4].

In figures 3.6 and 3.7, the measured stress-displacement is given together with the lines 1 and 2 according to eq.(3.17). The strain ε_g follows from the displacements at the *x*-axis of the figures divided through 3 mm, the measuring length and length of the specimen. Because of the small length of 3 mm, not the whole width *b* of the specimen is active. Assuming a possible spreading of 1.2:1, through the thickness of 1.25 mm above and below the side notches, the working width b_{eff} is equal to the length of the fracture plane plus 2 times 1.2 x 1.25 or b_{eff} = 10 + 3 = 13 mm. Thus the notch lengths in Figure 3.5 should be regarded to be 1.5 mm instead of 5 mm. The stresses in the figures 3.6 and 3.7 of [4], are related to the length of the fracture plane and not to b_{eff}, according to the Griffith stress. Thus the given stresses have to be reduced by a factor 10/13 = 0.77.

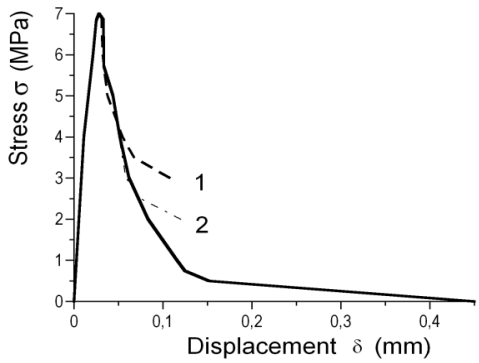

Figure3.6. Stress - displacement of specimen T 1409 of [4].

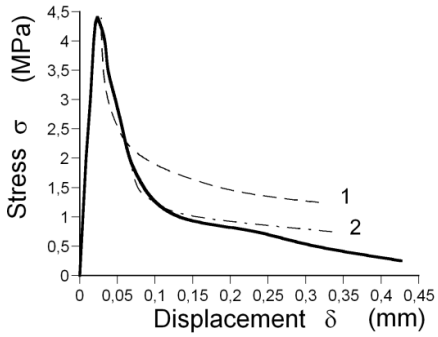

Figure3.7. Stress - displacement of specimen T 1509 of [4].

The standard compact tension tests of [4] did show a stress intensity K_{Ic} of 330 $\mathrm{kNm}^{-3/2}$. This result is independent on the chosen stiffness as follows from the calculation according to the series solution or according to the energy method. This is verified in [4] by comparing the series solution with a finite element compliance calculation using the isotropic and theorthotropic stiffness and the quite different orthotropic stiffness of [5]. The value of K_{Ic} = 330 $\mathrm{kNm}^{-3/2}$, found in all cases, thus also should follow from the area under the softening curve of that compact tension test. When half the area of that diagram is taken to be the fracture energy, instead of the total area, then K_{Ic}, mentioned in [4], indeed is corrected to the right value of: 467/√2 = 330 $\mathrm{kNm}^{-3/2}$, giving the first empirical verification of the theory.

Regarding the short double edge notched specimens of Figure3.5, the measured E-modulus should be related to the effective width of 13 mm instead of the width of 10 mm of the fracture plane and therefore is *E* = 700x10/13 = 700x0.77 = 539 MPa. The critical energy release rate then is:

$$G_c = K_{Ic}^2 / E = 330^2 / 539 = 200 \text{ N/m} \tag{3.20}$$

The measured value of G_c from the area under the stress-displacement curve is given in [4] to be 515 N/m. But, because half this area should have been taken and this value is wrongly related to the length of the fracture plane instead of on b_{eff}, the corrected value is:

$$G_c = 1/2\text{x}515\text{x}0.77 = 200 \text{ N/m}, \tag{3.21}$$

as found above, eq.(3.20), giving again an empirical verification of the theory, now by the tests on the short double edge notched specimens.

As shown before, the softening curve of Figure3.6 has a vertical tangent at the top $d\sigma_g / d\varepsilon_g = \infty$. The critical crack length for softening is: $c_c = \sqrt{bl / 6\pi}$ according to eq.(3.13). Thus:

$$c_c = \sqrt{\frac{b_{eff} l}{6 \cdot \pi}} = \sqrt{\frac{13 \cdot 3}{6 \cdot \pi}} \cdot 10^{-3} = 1.4 \cdot 10^{-3} = 1.4 \text{ mm} \tag{3.22}$$

This confirms the mentioned initial St. Venant crack length of the specimen to be as small as about 1.5 mm.

In Figure3.6, at the Griffith maximal stress of (0.77)·7 = 5.39 MPa, is: $K_{Ic} = \sigma\sqrt{\pi c}$ or:

$$\mathrm{K_{Ic}} = 5.39 \cdot \sqrt{\pi \cdot 1.4 \cdot 10^{-3}} = 0.36 \ \mathrm{MNm}^{-3/2}. \tag{3.23}$$

Thus above the mean value of 0.33 $\mathrm{MNm}^{-3/2}$ for this strong specimen.

Line 1 of Figure3.6 gives the primary crack extension, eq.(3.17), with σ_c = (0.77)·7 = 5.39 MPa and a displacement of about 0.03 mm, (or a strain of 0.03/3 = 0.01). The strength of the fracture plane of 7 to 8 MPa is rather high and only measured 6 times of the 117 tests. The crack does not propagate in a free space, but in the limited length of the fracture plane and this area will be overloaded. Curve 1 therefore levels off from the measurements at σ = 0.77·4 MPa. Thus:

$$\sigma_g = \sqrt{\frac{EG_c}{\pi 3c_c}} = 0.57\cdot(0.77\cdot 7) = 0.77\cdot 4 \text{ MPa} \qquad (3.24)$$

Thus this happens when the crack length has become about 3 times the initial critical value $c_{c,0}$. The remaining intact length of the fracture plane then is: 4.4 mm or 4.4/13 = 0.34, while the remaining intact length is 5 mm for small-crack pattern A (of Section 3.6), or 5/13 = 0.38. Thus less fracture energy is required for small-crack failure and it thus is probable that macro-crack extension is always due to small-crack propagation toward the macro-crack tip. The level above 4 (to 4.6) MPa is measured in 3 of the 10 specimens of the discussed series T1309/2309 of [4] and an example is given in Figure3.7. The other specimens of this series did show lower strength values than 4 MPa, indicating that this strength of the fracture plane according to crack-pattern A was determining for softening. The same applies for further softening. The transition to crack pattern B and to pattern C is according to eq.(3.18), verified by eq.(3.19), showing that in Figure3.6, σ_c is constant and equal to σ_c/0.77 = 7 MPa for σ_g/0.77 = 7 down to σ_g/0.77 = 4 MPa and then reduces gradually to σ_c/0.77 = 4.5 at σ_g/0.77 = 2 and further to σ_c/0.77 = 3 at σ_g/0.77 = 1 MPa. The same applies for Figure3.7, σ_c/0.77 = 7 MPa above σ_g/0.77 = 4 MPa and then reduces in the same way. These results are given in Table 1. The departure from the Griffith theory by the gradual decrease of σ_c, below σ_g/0.77 = 4 MPa, is due to the failure of the high loaded fracture plane what is explained in the next section.

3.6. Crack Joining Mechanism

The discussed apparent decrease of the fracture energy G_c of the Griffith theory, due to reduction of intact area of the fracture plane of the specimen by small crack extensions at the fracture plane, can be explained, using the equilibrium method, by the joining of the small cracks as follows:.

In [3] it is shown that the critical intermediate small crack distance of a fracture process in “clear” wood, and thus in the fracture plane, is about equal to the crack length, as given in scheme A below. In Section 3.3, a crack distance of 2.2 times the crack length is found, what for simplicity of the model is rounded down here to 2, giving slightly too high stresses (see Table 1). For these small cracks, the critical crack length according to eq.(3.13) then is:

2c 2c 2c 2c 2c 2c 2c 2c 2c 2c 2c 2c 2c 2c . A

6c 2c 6c 2c 6c 2c 6c . B

14c 2c 14c . C

$c_c = \sqrt{lb/6\pi} = \sqrt{2\cdot(2c_0)\cdot 2\cdot(2c_0)/(6\pi)} = 0.92\cdot c_0 \approx c_0$, for the specimen with row A.

The distance l between the rows, above each other, is always two times the crack length, being the Saint-Venant distance for building up the stress again behind a crack to be able to form a new crack. Thus $l = 2\cdot 2c$ for row A, and $l = 2\cdot 6c = 12c$ in row B, and $2\cdot 14c = 28c$ in row C. The crack distance b in row A is $b = 4c$, and b = $8c$ in row B, and $16c$ in row C. Thus when crack pairs of row A join together, a crack length of $6c$ occurs, at a distance $8c$, and so on. The critical crack length thus is for row B:

$c_c = \sqrt{lb/6\pi} = \sqrt{12\cdot 8\cdot c_0^2/(6\pi)} = 2.26\cdot c_0$ and is

$c_c = \sqrt{lb/6\pi} = \sqrt{28\cdot 16\cdot c_0^2/(6\pi)} = 4.88\cdot c_0$ for row C.

The critical stress σ_c is for row A:

$$\sigma_c = \sqrt{\frac{EG_c}{\pi 0.92 c_0}} = 1.04\cdot\sqrt{\frac{EG_c}{\pi c_0}} = 1.04\cdot\sigma_{cm} \approx 1.0\cdot 0.77\cdot 7 = 0.77\cdot 7.0 \text{ MPa},$$

and for row B:

$$\sigma_c = \sigma_{cm}\cdot\left(1/\sqrt{2.26}\right) = \sigma_{cm}\cdot 0.67 = 0.67\cdot 0.77\cdot 7 = 0.77\cdot 4.6 \text{ MPa},$$

and for row C:

$$\sigma_c = \sigma_{cm}\cdot\left(1/\sqrt{4.88}\right) = \sigma_{cm}\cdot 0.45 = 0.45\cdot 0.77\cdot 7 = 0.77\cdot 3.1 \text{ MPa}$$

The determining strength of the intact part of the fracture plane is:

$\sigma_m = \sigma_u\cdot 2c/b = \sigma_u\cdot 2c/4c = \sigma_u/2 = 4\cdot 0.77$ MPa for case A;

$\sigma_m = \sigma_u\cdot 2c/8c = \sigma_u/4 = 2\cdot 0.77$ MPa for case B, and

$\sigma_m = \sigma_u\cdot 2c/16c = \sigma_u/8 = 1\cdot 0.77$ MPa for case C.

Thus the decrease of the Griffith values σ_c and G_c is fully explained by the strength of the intact part of the fracture plane $\sigma_g = \sigma_m$ as is verified by the measurements. As mentioned before, eq.(3.19) of σ_c, of the softening curve gives the measurement of Figure3.6 and 3.7 in the first two columns of Table 1, together with the prediction of the crack joining mechanism in column 5 and 6. This mechanism thus precisely explains the decrease of σ_c of the softening curve, which also can be approximated by three equations (3.18) for the 3 critical crack densities A, B and C. The strength decrease by a factor 0.5 between these crack densities in column 6 causes a decrease of the top-value σ_c of eq.(3.17) of a factor 0.657 in column 1 and 5. Thus: 0.657·7 = 4.6 and 0.657·4.6 = 3. Thus a simple practical approximation of the mean softening curve of all specimens of the series, is possible by applying eq.(3.17) twice (or three times for the highest values), according to line 1 and 2 in Figure 3.6 and 3.7.

Table 1. Softening by macro crack propagation followed by fracture plane failure

eq.(3.19), data Figure 3.6				crack joining	
$\sigma_c / 0.77$ eq.(3.19)	$\sigma_g / 0.77$ Chosen points	σ_g / σ_{g1} data	$\varepsilon_g / \varepsilon_{g1}$ data	$\sigma_c / 0.77$ 3 crack densities	$\sigma_m / 0.77$ strength fract.plane
7	7				
7	4	4/7	7.5/4	7	A: 4
4.6	2	2/7	11.5/4	4.6	B: 2
3.0	1	1/7	16/4	3.1	C: 1

The analysis above shows that in general:

$2c_{n+1} = 2 \cdot 2c_n + 2c_0$, giving $2c_1 = 6c_0$ and $2c_2 = 2 \cdot 2c_1 + 2c_0 = 14c_0$.

The increase of the crack length is: $\Delta(2c)' = 2c_{n+1} - 2c_n = 2c_n + 2c_0$. Including the initial crack length of $2c_0$, the increase of the total crack length is:

$$\Delta(2c) = 2c_{n+1} - 2c_n - 2c_0 = 2c_n . \tag{3.25}$$

More general for any crack distance this is: $\Delta(2c) = \beta_1 \cdot 2c$ and because the strength decrease is proportional to the area decrease of the fracture plane area of the test specimen, due to the small cracks extension there, the equation becomes:

$$\Delta(2c)/(2c) = -\beta_2 \cdot \Delta(G_c) \tag{3.26}$$

giving the explanation of the decrease of σ_c.

Eq.(3.26) also can be expressed in the mean crack velocities by replacing c by $\dot{c}t$, the mean crack velocity $\dot{c}$ times time t. Thus: $\Delta(2c)/(2c) = \Delta(\dot{c}t)/\dot{c}t = \Delta\dot{c}/\dot{c}$. Then integration of eq.(3.26) leads to:

$$G_{c,a} = G_{c,a,1} - \gamma \cdot \ln(\dot{c}), \tag{3.27}$$

This is measured in [2] and mentioned in [6] for the irreversible work of loading cycles.

It is shown in [3] that G is proportional to the activation energy and thus proportional to the driving force K_I with reversed sign and Eq.(3.27) can be written relative to a reference $\dot{c}_m$:

$$\frac{\sigma_t}{\sigma_{t,m}} = 1 + \frac{1}{n}\ln\left(\frac{\dot{c}}{\dot{c}_m}\right) = \frac{K_I}{K_{I,m}} \tag{3.28}$$

This semi log-plot, eq.(3.28), is given, as empirical line, in many publications from experiments on, e.g., ceramics, polymers, metals and glasses, and is, e.g., given in [6] for wood. Because the slope is small, also the empirical double log-plot is possible.

The kinetics shows the same behaviour as for clear wood indicating that small-crack propagation is always determining. As shown in [1], two coupled processes act, showing the same time-temperature and time-stress equivalence. One process, with a very high density of sites, provides the sites of the second low site density process, as follows from a very long delay time of the second process. The notched specimen discussed here also shows the low concentration reaction by the strong softening behaviour. Probably the coupled processes are the numerous small-cracks growing towards the macro notch, providing the site for the macro crack to grow as second low (crack-) concentration process. This failure mechanism thus applies for every bond breaking process at any level.

3.7. References

[1] T.A.C.M van der Put, *Deformation and damage processes in wood*, Delft University Press, The Netherlands, (1989).

[2] Y.W. May, On the velocity-dependent fracture toughness of wood, *Wood Science*, July 1975

[3] T.A.C.M van der Put, A new fracture mechanics theory of orthotropic materials like wood, *Engin. Fract. Mech*. 74/5 (2007) pp 771-781.

[4] L. Bostrom, Method for determination of the softening behaviour of wood etc. Thesis, Report TVBM-1012, Lund, Sweden, (1992).

[5] G.C. Sih, P.C. Paris and G.R. Irwin, On cracks in rectilinearly anisotropic bodies, *Int. J. of Fract. Mech.* 1 (1965) 189-203.

[6] G.H. Valentin, L. Bostrom, P.J. Gustafsson, A. Ranta-Maunus, S. Gowda, RILEM state-of-the-art report on fracture mechanics, VTT Report 1262, Espoo, Finland July 1991

4. DISCUSSION OF THE FRACTURE MECHANICS MODELS APPLIED TO WOOD

4.1. Introduction

The always applied singularity approach of fracture mechanics contains no physical failure criterion for the ultimate state because stresses go to infinity at the singularity and therefore energy methods are necessary and additional models to constitute such failure criteria as for instance the J-integral to determine the strain energy release rate and the fictitious crack models to obtain finite ultimate stresses etc. The general applicability of these models will be discussed in this section while criteria based on a critical energy are discussed in the next section.

4.2. The Fictitious Crack Models

The high stresses near the crack tip, are replaced by a plastic zone in the Dugdale model following from elastic superposition of closing stresses, equal to the yield stress, on the crack tip zone of a fictitious enlarged crack of such a length that the stress in the elastic singularity point becomes zero. The length of that plastic zone is r_p according to:

$$r_p = \frac{\pi}{8} \cdot \left(\frac{K_{Ic}}{\sigma_f} \right)^2 = \frac{\pi^2 \sigma^2 c}{8\sigma_f^2} \tag{4.1}$$

where σ_f is the yield stress or is regarded to be a cohesive stress.

This leads to a maximal crack opening displacement δ_c at the crack tip of:

$$\delta_c = \frac{8}{\pi E} \cdot \sigma_f \cdot r_p = \frac{K_{Ic}^2}{E\sigma_f} = \frac{\pi \sigma^2 c}{E\sigma_f} \tag{4.2}$$

when r_p from eq.(4.1) is substituted.

According to the theory of Section 2 applies, for Mode I, at the crack tip boundary r_0, at the start of flow, the condition: $r_0 = 2c\left(\sigma / \sigma_f\right)^2$ according to eq.(2.29) for the elliptic crack tip and approximately $r_0 = c\sigma^2 / 2\sigma_f^2$ according to eq.(2.20) for the circular crack tip,

showing a difference by a factor 4, depending on the form of the crack tip and thus depending on the value of the tangential tensile stress along the crack-tip boundary. The Dugdale numerical factor $\pi^2/8 = 1.23$ is between the values of 0.5 and 2 but is too far away from the elliptic value 2 which applies generally. Also the theoretical elastic elliptic crack opening displacement of $\delta_c = (2\sigma c)/E$ is far above the Dugdale value. The Dugdale model thus is a model according to the equilibrium method, based on a chosen, allowable equilibrium system, providing however a too low and thus rejectable lower bound with respect to the theoretical description of Section 2. The same applies for the Hillerborg model which is not based on a constant closing stress σ_f, but on closing stresses proportional to the softening curve. This of course is not right because there is no softening at the fracture plane. The real stress in the intact area is the ultimate yield stress and yield drop thus is a system property indicating how much broken area with zero stress there is in the fracture plane (see Section 3).

For wood it is sufficient to account for apparent plasticity zones around the crack-tip by regarding effective crack dimensions and to regard the critical state at these elastic-"plastic" boundaries.

4.3. Crack Growth Models

The acknowledged, in principle identical crack growth models for wood of Williams, Nielsen and Schapery, mentioned in [1], are based on linear viscoelasticity and on the Dugdale-Barenblatt model in order to try to derive the empirical crack rate equation:

$$\frac{da}{dt} = A \cdot K_I^n \tag{4.3}$$

This procedure is contrary to normal and can not lead to a real solution because the rate equations are constitutive and follow from Deformation kinetics theory [2], [3], as applies for all materials. Constitutive equations only can follow from the theory and not from general thermodynamic considerations.

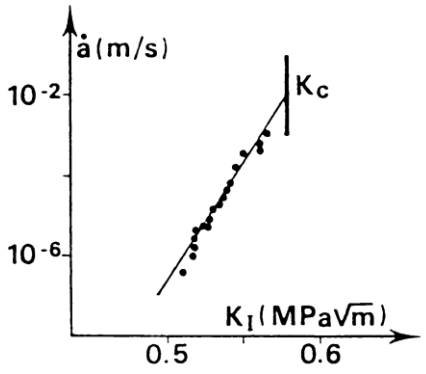

Figure 4.1. Crack growth tests of Mindess (Figure 10 of [1]).

In [1] is stated that Fig 4.1 represents eq.(4.3). However, eq.(4.3) is a straight line on a double log-plot, while Figure 4.1 gives the semi-log-plot which confirms the applicability of the damage equation of Deformation Kinetics [2] in the form: $\dot{a} \approx C \cdot \exp(\phi\sigma_v)$, or:

$$\ln(\dot{a}) = \ln(C) + \phi\sigma_v \tag{4.4}$$

This equation is equal to eq.(3.28), discussed in Section 3. More appropriate forms of theexact damage equations and power law forms, with the solutions as e.g. the yield drop in the constant strain rate test, are discussed in [2] and the meaning of the power law equation, eq.(4.3), is discussed below.

The impossibility of the derivation of the fracture rate equation from the Dugdale-Barenblatt equations follows e.g. from the derivation in [6, Section 2.2] of eq.(4.5):

$$K_{Ic} = E_0 \cdot \dot{a}^n \cdot \sqrt{\delta_c \varepsilon_y} \cdot r_p^{-n} \tag{4.5}$$

based on the relations: $\varepsilon_y = \sigma_c / E$ and $K_{Ic} = \sqrt{E\sigma_c\delta_c}$, with $E = E_0 \cdot t^{-n}$ and $r_p = \dot{a} \cdot t$. These four relations thus also can be used now to eliminate 4 parameters, e.g. K_{Ic}, ε_y, r_p and E_0 to obtain an equation in *E*, *t*, $\dot{a}$ σ_c and δ_c. When this is done, eq.(4.5) turns to an identity: *E* = *E*, and eq.(4.5) thus is not a new derived crack rate equation but an alternative writing of the four relations. The same follows for the other models of Section 2.2 of [1] showing comparable parameter manipulations of many critical parameter values which can not be applied independently because they are part of the same failure condition. The models further are based on linear viscoelasticitywhich does not exist for polymers. It is shown in e.g. [2], page 97, and by the zero creep and relaxation tests at page 119, that a spectrum of retardation or relaxation times does not exist. The superposition integral eq.(28) or eq.(51) of [1]:

$$\varepsilon(t) = \int_{-\infty}^{t} C(t-\tau)\frac{d\sigma(\tau)}{d\tau}\,d\tau \tag{4.6}$$

thus has no physical meaning. This also applies for the power law models of time and power law equation, eq.(4.3) making predictions and extrapolations outer the fitted range of the data impossible.

4.4. Derivation of the Power Law

The power law may represent any function f(x) as follows from the following derivation. It thus also may represent, in a limited time range, a real damage equation giving then a meaning of the power *n* of the power law eq.(4.3).

Any function *f(x)* always can be written in a reduced variable x/x_0

$$f(x) = f_1(x/x_0) \tag{4.7}$$

and can be given in the power of a function:

$f(x) = f_1(x/x_0) = \left(\left(f_1(x/x_0) \right)^{1/n} \right)^n$ and expanded into the row:

$$f(x) = f(x_0) + \frac{x - x_0}{1!} \cdot f'(x_0) + \frac{(x - x_0)^2}{2!} \cdot f''(x_0) + ...$$

giving:

$$f(x) = \left[\left\{ f_1(1) \right\}^{1/n} + \frac{x - x_0}{x_0} \frac{1}{n} \left\{ f_1(1) \right\}^{1/n-1} \cdot f'(1) + ... \right]^n = f_1(1) \cdot \left(\frac{x}{x_0} \right)^n \tag{4.8}$$

when:

$$\left(f_1(1) \right)^{1/n} = \frac{1}{n} \left(f_1(1) \right)^{1/n-1} \cdot f'(1) \quad \text{or: } n = f_1'(1) / f_1(1),$$

where:

$$f_1'(1) = \left(\partial f_1(x/x_0) / \partial (x/x_0) \right)_{(x/x_0)=1}$$

and

$$f_1(1) = f(x_0)$$

Thus:

$$f(x) = f(x_0) \cdot \left(\frac{x}{x_0} \right)^n$$

with

$$n = \frac{f_1'(1)}{f_1(1)} = \frac{f'(x_0)}{f(x_0)} \tag{4.9}$$

It is seen from this derivation of the power law, using only the first 2 expandedterms, that the equation only applies in a limited range of *x* around x_0.

Using this approach on the damage equation: $\dot{a} = 2C \cdot \sinh(\phi\sigma) \approx C \exp(\phi\sigma)$ gives:

$$\dot{a} = C \cdot \exp(\phi\sigma) \approx \dot{a}_0 \cdot \left(\frac{\sigma}{\sigma_0} \right)^{\phi\sigma_0} \tag{4.10}$$

The power $n = \phi\sigma_0$ of the power law equation follows from the slope of the double log-plot:

$$\ln(\dot{a}) = \ln(\dot{a}_0) + n \cdot \ln(\sigma / \sigma_0) \tag{4.11}$$

Thus: $n = d\ln(\dot{a}) / d\ln(\sigma / \sigma_0)$ and $n = \phi\sigma_0$ gives a meaning of *n* as the activation volume parameter $\phi\sigma_0$ of the exact equation. The values of "*n*" and the matching activation energies of the different creep and damage processes in wood, with the dependency on stress moisture content and temperature, are given in [2]. The constancy of the initial value of the parameter $\phi\sigma_0$, independent of σ_0 explains the time-temperature and time- stress equivalence and explains, by the physical processes, why and when at high stresses, the in [1] mentioned value of $n + 1 \approx 60$ is measured and at lower stresses, half this value (see [2]).

4.5. References

[1] RILEM state of the art report on fracture mechanics, Espoo, 1991.
[2] van der Put, T.A.C.M., *Deformation and damage processes in wood*, Delft University press, 1989.
[3] van der Put, T.A.C.M., Transformations in wood, Delft University, *Stevin-laboratory Research Report*, 2003-3/ME-2.

5. ENERGY THEORY OF FRACTURE

5.1. Introduction

The failure criterion of clear wood, i.e. wood with small defects, is the same as the failure criterion of notched wood, showing again that the small-crack extension towards the macro-crack tip is the cause of macro-crack propagation. This small-crack failure criterion thus delivers essential information on macro-crack behaviour.

5.2. Critical Distortional Energy as Fracture Criterion

The failure criterion of wood consist of an orthotropic third degree tensor polynomial [1], which, for the same loading case, is identical to the Wu-mixed mode I-II-equation [2], eq.(5.3). The second degree polynomial part of the failure criterion is shown to be the orthotropic critical distortional energy principle for initial yield [3] showing the start of

dissipation of elastic distortional energy as also confirmed by the orthotropic finite element calculation of [4]. By this dissipation according to the incompressibility condition, the minimum energy principle is followed providing therefore the exact initial yield criterion as:

$$\frac{\sigma_x^2}{XX'}+\frac{\sigma_x}{X}-\frac{\sigma_x}{X'}-2F_{12}\sigma_x\sigma_y+\frac{\sigma_y^2}{YY'}+\frac{\sigma_y}{Y}-\frac{\sigma_y}{Y'}+\frac{\tau^2}{S^2}=1 \tag{5.1}$$

where X, Y are the tension strengths and X', Y' the compression strength in the main directions and S is the shear strength and: $2F_{12}=1/\sqrt{XX'YY'}$

This value of F_{12} is necessary for the elastic state which also applies at the starting point of initial stress redistribution and micro-cracking of the matrix. After further straining, F_{12} becomes zero, $F_{12}\approx 0$, at final failure initiation. The absence of this coupling term F_{12} between the normal stresses indicates symmetry, thus (possible random oriented) initial small-cracks are extended during loading to their critical length in the weak planes, the planes of symmetry, only. Then, when these small-cracks arrive at their critical crack-density (discussed in Section 3.6) and start to extend further, a type of hardening occurs because the reinforcement prevents crack extension in the matrix in the most critical direction. Then, due to hardening, F_{12} and all third degree coupling terms of the tensor polynomial become proportional to the hardening state constants [3] and therefore also dependent on the stability of the test and equipment. For the mixed I-II-loading of the crack plane by tension σ_2 and shear σ_6, the polynomial failure criterion reduces to:

$$F_2\sigma_2+F_{22}\sigma_2^2+F_{66}\sigma_6^2+3F_{266}\sigma_2\sigma_6^2=1 \quad \text{or:} \quad \frac{\sigma_6}{S}=\sqrt{\frac{(1-\sigma_2/Y)\cdot(1+\sigma_2/Y')}{1+c\sigma_2/Y'}} \tag{5.2}$$

with: $c=3F_{266}Y'S^2\approx$ 0.9 to 0.99, depending on the stability of the test. When c approaches $c\approx$ 1, Eq.(5.2) becomes Eq.(5.3), the in Section 2.3 theoretically explained Wu-equation, with a cut off by the line: $\sigma_2=Y$.

$$\left(\frac{\sigma_6}{S}\right)^2+\frac{\sigma_2}{Y}\approx 1 \quad \text{or:} \quad \frac{K_{II}^2}{K_{IIc}^2}+\frac{K_I}{K_{Ic}}=1 \tag{5.3}$$

This equation contains no hardening constants and thus is the critical distortional energy equation for this case. Wrongly for wood and other orthotropic materials, Eq.(5.2) is generally replaced in literature by:

$$\frac{\sigma_2^2}{Y^2}+\frac{\tau^2}{S^2}=1, \text{ written as: } \frac{K_I^2}{K_{Ic}^2}+\frac{K_{II}^2}{K_{IIc}^2}=1, \tag{5.4}$$

which surely is not a summation of energies, as is stated, but is identical to eq.(5.1) when it wrongly is assumed that the compression and tension strength are equal for wood and orthotropic materials.

5.3. Revision of the Critical Energy Release Rate Equation

Based on the failure criterion of Section 5.2, adaption of the energy release equation is necessary.

The Griffith strength equation, eq.(3.8) of Section 3: $\sigma_y^2 = G_c E_y / \pi c$ can be extended by superposition to:

$$\sigma_y^2 + \tau_{xy}^2 = G_c E_y / \pi c \tag{5.5}$$

This only is right, when G_c is not constant but depends on σ_y / τ_{xy}, because else, for σ_y = 0, Eq.(5.5) predicts a too low shear strength. This already was noticed by Griffith. The fracture toughness calculation of Section 2.3 shows a two times higher shear strength of the isotropic matrix than according to the energy method. This was explained by supposing that there is enough energy for failure, but that the shear stresses are too low for failure. Only the energy of high stresses is involved in failure. This however means that G_f also has to satisfy the failure condition eq.(5.3).

In orthotropic stresses, Eq.(5.5) is: $\sigma_y^2 + \tau_{xy}^2 / n_6^2 = G_f E_y / \pi c$ and when $\tau_{xy} = 0$, is

$G_f = G_{Ic}$

and $K_{Ic} = \sqrt{E_y G_{Ic}}$

When $\sigma_y = 0$ is: $\tau_{xy}^2 \pi c = n_6^2 G_{IIc} E_y = 4 n_6^2 G_{Ic} E_y$, because

$K_{IIc} = 2 n_6 K_{Ic}$ (eq.(2.37)). Thus: $K_{IIc} = n_6 \sqrt{E_y G_{IIc}} = 2 n_6 \sqrt{E_y G_{Ic}}$ or:

$$G_{IIc} = 4 G_{Ic} \tag{5.6}$$

The failure condition Eq.(5.3) can be written in fracture energies:

$$\frac{K_I}{K_{Ic}} + \frac{\left(K_{II}\right)^2}{\left(K_{IIc}\right)^2} = 1 = \frac{\sqrt{G_I}}{\sqrt{G_{Ic}}} + \frac{G_{II}}{G_{IIc}} = \frac{\sqrt{\gamma \cdot G_f}}{\sqrt{G_{Ic}}} + \frac{\left(1-\gamma\right) \cdot G_f}{G_{IIc}} \tag{5.7}$$

where:

$$G_f = G_I + G_{II} = \gamma \cdot G_f + (1-\gamma) \cdot G_f \tag{5.8}$$

Thus: $\dfrac{\gamma G_f}{(1-\gamma) G_f} = \dfrac{K_I^2}{K_{II}^2}$ or: $\gamma = \dfrac{1}{1+\dfrac{K_{II}^2}{K_I^2}} = \dfrac{1}{1+\dfrac{\tau_{xy}^2}{\sigma_y^2}}$ (5.9)

and γ depends on the stress combination τ_{xy} / σ_y in the region of the macro notch-tipand not on the stresses of the fracture energy. This stress combination may follow from a chosen stress field according to the equilibrium method as applied in Section 6 and 7.

With eq.(5.6): $G_{IIc} / G_{Ic} = 4$, eq.(5.7) becomes:

$$G_f = 4G_{Ic} / (1+\sqrt{\gamma})^2 = G_{IIc} / (1+\sqrt{\gamma})^2 \tag{5.10}$$

The use of G_f according Eq.(5.10) explains the differences in fracture energies depending on the notch depth and structure and shear slenderness of the beam by the different occurring τ_{xy} / σ_y -values according to Eq.(5.9).

Applications of the theory with the total critical fracture energy G_f are given in Section 6 and 7.

5.4. References

[1] van der Put, T.A.C.M. (1982) A general failure criterion for wood, CIB-W18/IUFRO meeting Boras, Sweden

[2] Wu, E.M. (1967) Application of fracture mechanics to anisotropic plates, *ASME J. Appl. Mech*. Series E, 34 4, pp. 967-974.

[3] van der Put T.A.C.M. (2009) A continuum failure criterion applicable to wood. *J. of Wood Sci*, Vol. 55 No.5. (DOI: 10.1007/s10086-009-1036-2)

[4] Gopu, Vijaya K. A. (1987) Validity of Distortion-Energy-Based Strength Criterion for Timber Members, *J. Struc. Eng*. 113, No. 12 pp. 2475-2487.

6. ENERGY APPROACH FOR FRACTURE OF NOTCHED BEAMS

6.1. Introduction

The theory of total fracture energy, discussed in Section 5, was initially developed to obtain simple general design rules for beams with square end-notches and edge joints, loaded

perpendicular to the grain design rules of square notches and joints for the Dutch Building Code and later, as modification of the method of [1], published in [2] with the extensions for high beams. Horizontal splitting in short, high beams, loaded close to the support, causes no failure because the remaining beam isstrong enough to carry the load and vertical transverse crack propagation is necessary for total failure. This is not discussed here because it is shown that also the standard strength calculation is sufficient. In [3] and [4] the theory is applied to explain behaviour, leading to the final proposal for design rules for the Eurocode, given at Section 7.5, and to an always reliable simple design method.

In the following, the theoretical basis and implementation of the new developments of the theory of the energy approach for fracture of notched beams are given and it is shown that the predictions of the theory are verified by the measurements. The presentation of more data can be found in [2].

6.2. Energy Balance

When crack-extension occurs over the length Δx, along the grain, then the work done by the constant load V is $V{\cdot}\Delta\delta$, where $\Delta\delta$ is the increase of the deformation at V. This work is twice the increase of strain energy of the cantilever part: $V{\cdot}\ \Delta\delta/2$. Thus half of the external work done at cracking is used for crack formation being thus equal to the other half, the strain energy increase.

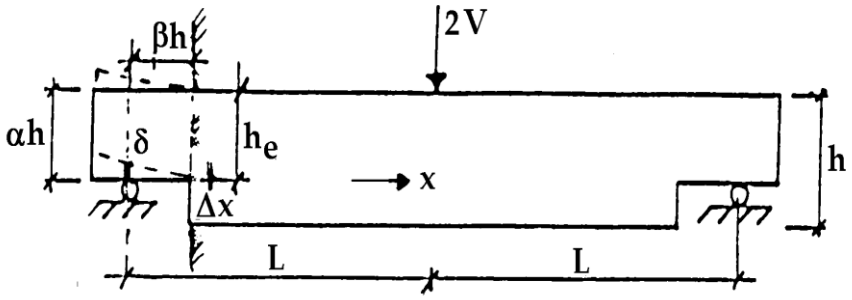

Figure 6.1. Notched beam.

Thus in general, when the change of the potential energy $\Delta W = V{\cdot}\Delta\delta/2$ becomes equal to the energy of crack formation, crack propagation occurs. The energy of crack formation is: $G_c b\Delta x = G_c bh\Delta\beta$, where G_c is the crack formation energy per unit crack area. Thus crack propagation occurs at $V = V_f$ when:

$$\Delta W = V\Delta\delta/2 = V^2\Delta(\delta/V)/2 = G_c bh\Delta\beta,$$

thus when:

$$V_f = \sqrt{\frac{2G_c bh}{\partial(\delta / V)/\partial\beta}} \tag{6.1}$$

and only the increase of the compliance δ/V has to be known.

The deflection δ can be calculated from elementary beam theory as chosen allowable equilibrium system as a lower bound of the strength. This is close to real behaviour because, according to the theory of elasticity, the deflection can be calculated from elementary beam theory while the difference from this stress distribution is an internal equilibrium system causing no deflection of the beam and also the shear distribution can be taken to be parabolic according to this elementary theory, as only component of this polynomial expansion, contributing to the deflection.

According to the Figure 6.2, the notch can be seen as a horizontal split, case: a = a', and case a can be split in the superposition of case b and c, where b = b'.

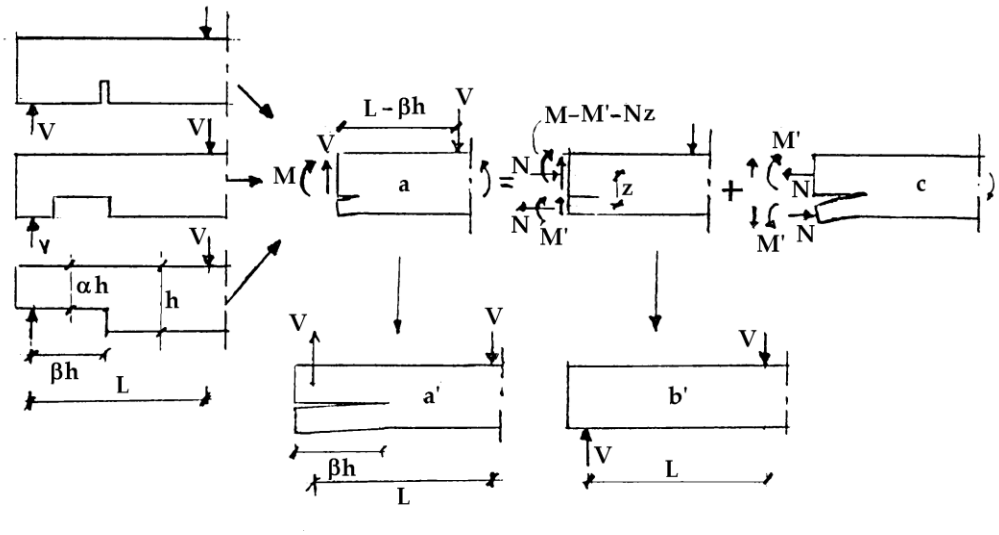

Figure 6.2. Equivalent crack problem according to superposition.

Case c now is the real crack problem by the reversed equal forces that can be analyzed for instance by a finite element method, etc. From the principle of energy balance it is also possible to find the critical value of case c by calculating the differences in strain energies or the differences in deflections δ by V between case: b' and case a', thus differences in deformation of the cracked and un-cracked part to find $\Delta(\delta/V)$ for eq.(6.1).

Deformations due to the normal stresses N of case c, are of lower order in a virtual work equation and should not be accounted. It then follows that case c of Figure 6.2 is equal to a mode I test and $G_c = G_{Ic}$. When the beam is turned upside down, or when V is reversed in direction, then M' and V' are reversed closing the crack and fracture only is possible by shear, identical to the mode II test and then $G_c = G_{IIc}$

The change of δ by the increase of shear deformation is, with $h_e = \alpha \cdot h$:

$$\delta_v = \frac{1.2}{G}\left(\frac{\beta h}{b\alpha h} - \frac{\beta h}{bh}\right)\cdot V \tag{6.2}$$

The change of δ by the increase of the deflection is:

$$\delta_m = \frac{V(\beta h)^3}{3Eb(\alpha h)^3/12} - \frac{V(\beta h)^3}{3Ebh^3/12} = \frac{4V\beta^3}{Eb}\cdot\left(\frac{1}{\alpha^3} - 1\right) \tag{6.3}$$

Thus:

$$\frac{\partial(\delta/V)}{\partial\beta} = \frac{1.2}{Gb}\cdot\left(\frac{1}{\alpha} - 1\right) + \frac{12\beta^2}{Eb}\cdot\left(\frac{1}{\alpha^3} - 1\right) \tag{6.4}$$

The critical value of V thus is according to eq.(6.1):

$$V_f = \sqrt{\frac{1.67G_c hb^2}{\frac{1}{G}\left(\frac{1}{\alpha} - 1\right) + \left(\frac{1}{\alpha^3} - 1\right)\cdot\frac{10\beta^2}{E}}} \tag{6.5}$$

or:

$$\frac{V_f}{b\alpha h} = \frac{\alpha\sqrt{GG_c/h}}{\sqrt{0.6(\alpha^3 - \alpha^4) + 6\beta^2\left(\alpha - \alpha^4\right)G/E}} \tag{6.6}$$

For small values of β eq.(6.6) becomes:

$$\frac{V_f}{b\alpha h} = \frac{\sqrt{GG_c/h}}{\sqrt{0.6\cdot(\alpha - \alpha^2)}} \tag{6.7}$$

For high values of β, eq.(6.6) becomes:

$$\frac{V_f}{b\alpha h} = \frac{\alpha\sqrt{EG_c/h}}{\beta\sqrt{6(\alpha - \alpha^4)}} \tag{6.8}$$

6.3. Experimental Verification

A verification of the prediction of the theory for high values β, eq.(6.8), when the work by shear is negligible, is given by Table 6.1 of an investigation of Murphy, mentioned in [1], regarding a notch starting at $\beta = 2.5$ and proceeding to $\beta = 5.5$. Further also beams were tested with a slit at a distance: $\beta = 2.5$. Because the exact eq.(6.6) gives a less than 1 % higher value, eq.(6.8) applies. ($\sqrt{GG_c}$ = 11.1 resp. 10.9 $\mathrm{N/mm^{1.5}}$) and: $\sqrt{EG_c}$ = 48.8 $\mathrm{N/mm^{1.5}}$. This value is used in table 6.1 for comparison of eq.(6.8) with the measurements, showing an excellent agreement between theory and measurement. For all specimens was: $\alpha = 0.7$; $\eta = L/h = 10$ (L is distance field loading to support) and b = 79 mm. The other values are given in table 6.1. The fracture energy is: $G_c = \left(48.8\right)^2 / 14000 = 0.17\mathrm{N/mm} = 170\,\mathrm{N/m}$, which agrees with values of the critical strain energy release rate. The value of K_{Ic} is about: $K_{Ic} \approx \sqrt{0.17 \cdot 700} = 10.9\ \mathrm{N/mm^{1.5}}$ = 345 $\mathrm{kN/m^{1.5}}$, as to be expected by the high density of Douglas fir.

Table 6.1. Strength of clear laminated Douglas firwith notches in the tensile zone in MPa

***h* mm**	β	**number**	***V/αbh* tests eq.(6.8)**	
305	2.5	2	0.46	0.47
305	5.5	2	0.24	0.22
457	2.5	2	0.38	0.38
457	5.5	1	0.16	0.17

In table 6.2, data are given of Spruce for low values of β, to verify the then predicted theoretical behaviour according toeq.(6.7) with energy dissipation by shear stresses only. It appears for these data that the difference between the mean values according to eq.(6.7) and eq.(6.6) are 10 % and thus not negligible small and also the values of eq.(6.6) are given to obtain a possible correction factor.

It follows from table 6.2 for Spruce that: $\sqrt{GG_c} = 6.8\,\mathrm{N/mm^{1.5}}$ or: $G_c = 6.8^2 / 500 = 0.092\mathrm{N/mm} = 92\mathrm{N/m}$.

For Spruce is K_{Ic} ≈ 6.3 to 7.6 according to [5], depending on the grain orientation and then also applies: $E_2 \approx G$ and: $K_{Ic} = \sqrt{E_2 G_c} = 6.8\ \mathrm{N/mm^{1.5}}$.

Although the fracture energy is shear-stress energy, failure still is by mode I (of Figure 6.2) and not by the shear mode II, as is supposed by other models. Thus the total work contributes to failure, whether it is bending stress energy (Table 6.1) or shear stress energy (Table 6.2)and $\gamma = 1$ (eq.(5.9) for failure of this type of notch by the high tensile stress perpendicular to the grain at the notch root.

In [2] more data are given regarding the strength of square notches. The size influence, or the influence of the height of the notched beam on the strength, is tested on beams with notch

parameters α = 0.5 and 0.75; β is 0.5 and heights $h = 50$, 100 and 200 mm with b = 45 mm at moisture contents of 12, 15 and 18%. The strength $\sqrt{GG_f}$ appeared to be independent ofthe beam depth as to be expected for macro crack extension along an always sufficient long fracture plane. The value of $\sqrt{GG_f}$ at moisture contents of resp. 12, 15 and 18% was resp.: 6.7; 7.7 and 8.0 $\mathrm{Nmm}^{1.5}$.

Table 6.2. Strength of notched beams, Spruce, Mohler and Mistler

h mm	α	β	η/α	b mm	n	V/bαh N/mm^2	var. coef. %	$\sqrt{GG_f}$	
								eq.(6.6)	eq.(6.7)
								N/mm$^{1.5}$	
120	.917	.25	3.4	32	6	2.36	11	(5.8)	(5.5)
	.833		3.8		27	1.93	15	6,4	6.1
	.75		4.2		43	1.68	19	6.6	6.2
	.667		4.7		14	1.52	18	6.5	6.1
	.583		5.4		10	1.5	18	6.8	6.3
	.5		6.3		49	1.59	18	7.4	6.7
	.333		9.5		10	1.48	16	7.0	5.9
mean								**6.8**	**6.2**
Testing time more than 1 min., m.c. 11%, ρ = 510 kg/m^3									

Higher values of $\sqrt{GG_f}$ of Spruce, given in [2], are possible for loads close to the support. Then horizontal splitting does not cause failure because the remaining beam is strong enough to carry the total load and the derivation is given by regarding vertical crack propagation necessary for total failure (bending failure of the remaining beam). For this mode I,

$\sqrt{GG_m} = 57.5\ \mathrm{N/mm}^{1.5} = 1818\ \mathrm{kN/m}^{1.5}$ (comparable with 1890 $\mathrm{kN/m}^{1.5}$ of[5])

For still higher values of α, above α = 0.875, compression with shear failure is determining by direct force transmission to the support. In [3] is shown that Foschi's finite element prediction and graphs, given in [5] can be explained and are identical to eq.(6.8).

6.4. References

[1] P.J. Gustafsson, A Study of Strength of Notched Beams, CIB-W18A-21-10-1, meeting 21,Parksville, Vancouver Island, Canada, Sept. 1988.

[2] T.A.C.M. van der Put, Tension perpendicular to the grain at notches and joints. CIB-W18A-23-10-1, meeting 23, Lisbon, Portugal, Sept. 1990

[3] T.A.C.M. van der Put, Modified energy approach for fracture of notched beams. Proceed. COST 508 conf. on fracture mechanics. Bordeaux, April 1992.

[4] T.A.C.M. van der Put, A.J.M. Leijten, Evaluation of perpendicular to the grain failure of beams, caused by concentrated loads of joints. CIB-W18A/33-7-7, meeting 33, Delft, The Netherlands, August 2000.
[5] RILEM state of the art report on fracture mechanics, Espoo, 1991.

7. ENERGY APPROACH FOR FRACTURE OF JOINTS LOADED PERPENDICULAR TO THE GRAIN

7.1. Introduction

As for square end-notches, the analysis can be based on the compliance change by an infinitesimal crack increase. Because measurements show no difference in strength and fracture energy between joints at the end of a beam (Series G6.1 and G6.2 of [1]) and joints in the middle of the beam (the other G-series), and also the calculated clamping effect difference by crack extension is of lower order, this clamping effect of the fractured beam at the joint in the middle of a beam, has to be disregarded as necessity of the virtual energy equation of fracture. This is according to the limit state analysis which is based on the virtual work equations. For end-joints, the split off part is unloaded and there is no normal force and no vierendeel-girder action at all and the situation and fracture equations are the same as for the notched beams of Section 6. For joints in the middle of the beam, splitting goes in the direction of lower moments and is stable until the total splitting of the beam. The analysis in [1] and [2] shows this stable crack propagation because the terms in the denominator become smaller at crack length increase, until the shear term remains, giving the maximal value of V according to eq.(7.6), the same value as for end-joints.

It thus is not true, as is stated in the CIB/W18-discussion of [1], that the analysis and theory are incorrect when virtual lower order terms are omitted in the analysis and that splitting of joints analysis is not comparable to splitting of notched beam analysis. The proof that this neglecting of the vierendeel-action is right is (outer the empirical proof by the measurements) given by the complete analysis for this case in [3], where also the influence on the strain of normal stresses is accounted, leading to eq.(7.5) containing the negligible clamping effect term in the denominator, (based on the assumption that not total splitting of the beam is the end state).

7.2. Energy Balance

For a simplecalculation of the compliance difference of the cracked and un-cracked state, (maintaining the clamping action in the end state) half a beam is regarded, as given in Figure 7.1, loaded by a constant load V. At the start of cracking, the deflection at V increases with δ (see Figure 7.2) and the work done by the force V is: $2\Delta W = V \cdot \delta$, which is twice the increase of the strain energy ($\Delta W = V \cdot \delta/2$) of the beam and therefore the amount ΔW is used to increase the strain energy and the other equal amount of ΔW is used as fracture energy. Because δ is the difference of the cracked and "un-cracked" state, only the deformation of the cracked part βh minus the deformation of that same part βh in the un-cracked state, need to be

calculated, because the deformation of all other parts of the beam by load V are the same in cracked and un-cracked state. As discussed at 6.2, the deflection δ can be calculated from elementary beam theory of elasticity. It thus is not right to regard an additional deformation δ_r, as is done, due to the non-linearity and clamping effect of the cantilevers *βh*, formed by the crack. The clamping effect change is of lower order at aninfinitesimal crack extension. If this effect would have an influence, there should be a difference in notched beams in the splitting force for a real square notch of length *βh* and a vertical saw cut at a distance *βh* from the support, because that slit has at least twice that clamping effect (see Figure 6.2).

For a connection at the middle of a beam the following applies after splitting (see Figure 7.1). The part above the crack (stiffness $I_2 = b(1-\alpha)^3 h^3/12$) carries a moment M_3 and normal force N and the part below the crack (stiffness $I_1 = b\alpha^3 h^3/12$) carries a moment M_1, normal force N and a shear force V. and at the end of the crack a negative moment of about: $M_2 \approx -M_1$. Further is $M_2 = M_1 - V\lambda$, thus $M_1 = V\lambda/2$.

The deformation of beam 2 of the cracked part *βh* is equal to the un-cracked deformation δ_{un} of that part and the deformation of beam 1 is δ_{un} plus the crack opening δ (see Figure 7.1 and 7.2) and δ is:

$$\delta = \frac{1}{2}\cdot\frac{V\lambda^2}{EI_1}\cdot\frac{2}{3}\cdot\lambda - \frac{1}{2}\frac{M_1\lambda^2}{EI_1} = \frac{1}{3}\cdot\frac{V\lambda^3}{EI_1} - \frac{1}{4}\cdot\frac{V\lambda^3}{EI_1} = \frac{1}{12}\cdot\frac{V\lambda^3}{EI_1} = \frac{V\beta^3}{bE\alpha^3} \tag{7.1}$$

The deflection difference of the cracked and un-cracked state is total:

$$\delta = \frac{1.2}{G}\left(\frac{\beta h}{b\alpha h} - \frac{\beta h}{bh}\right)\cdot V + \frac{V\beta^3}{bE\alpha^3} \tag{7.2}$$

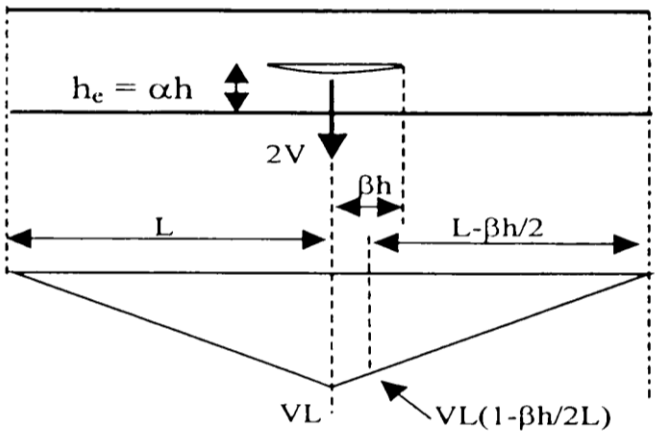

Figure 7.1. Beam with crack by the dowel force of a joint and bending moment.

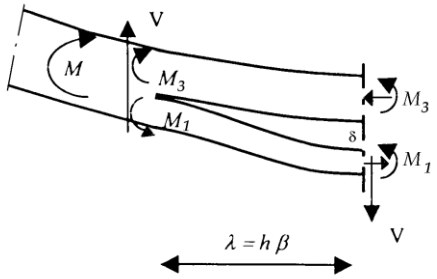

Figure 7.2. Statics of half the crack.

The condition of equilibrium at crack length β is:

$$\partial\left(V\cdot\delta/2-G_c b\beta h\right)/\partial\beta=0 \quad \text{or:} \quad \left\{\partial\left(\delta/V\right)/\partial\beta\right\}\cdot V^2/2=G_c bh$$

or:

$$V_f=\sqrt{\frac{2G_c bh}{\frac{\partial(\delta/V)}{\partial\beta}}} \tag{7.3}$$

where G_c is the fracture energy. It follows from eq.(7.2) that:

$$\frac{\partial\left(\delta/V\right)}{\partial\beta}=\frac{1.2}{bG}\left(\frac{1}{\alpha}-1\right)+\frac{3\beta^2}{Eb\alpha^3} \tag{7.4}$$

and eq.(7.3) becomes:

$$V_f=b\alpha h\sqrt{\frac{GG_c/h}{0.6\left(1-\alpha\right)\alpha+1.5\beta^2 G/(\alpha E)}} \tag{7.5}$$

giving, for the always relatively small values of β, the previous found eq.(6.7):

$$\frac{V_f}{b\alpha h}=\frac{\sqrt{GG_c/h}}{\sqrt{0.6\cdot(1-\alpha)\cdot\alpha}} \tag{7.6}$$

which thus also applies for notched beams and for end-joints and verifies the lower bound of the strength, predicted by the theory of [1]. This also indicates that only work by shear stresses contributes to fracture. The fit of the equation with vierendeel action, eq.(7.5), to the data is not better than the fit by eq.(7.6) what shows that the term $1.5\beta^2 G/\alpha E$ is small with respect to $0.6(1-\alpha)\alpha$ and also that β is about proportional to α and is of the same order. Comparison of eq.(7.5) and eq.(6.6) shows that the higher value of the end joint is

determining for this definition of the strength and the same design rules as for notches are possible for joints when not the joint but splitting is determining. However design should be based on "flow " of the joint before splitting of the beam and the interaction of joint failure and beam splitting has to be regarded as follows.

When crack extension starts of a cantilever beam loaded by a constant load *V*, giving a deflection increase of δ at *V*, then the applied energy to the beam is $V{\cdot}\delta$. The energy balance equation then is:

$$V\delta = V\delta/2 + E_c \tag{7.7}$$

where $V\delta/2$ is the increase of the elastic energy and E_c the energy of crack extension.

Thus: $E_c = V\delta/2$ (7.8)

Thus the energy of crack extension is equal to the increase of elastic energy.
Eq.(7.8) also can be written with de incremental deflection δ = d*u*:

$$E_c = V^2\,\mathrm{d}(u/V)/2 = = G_f bh\,\mathrm{d}(\beta)$$

or:

$$V = \sqrt{\frac{2G_f bh}{\partial(u/V)/\partial\beta}} \tag{7.9}$$

where G_f is the fracture energy per unit crack surface and "*bh*d*(β)*" the crack surface increase with "*b*" as width and "*h*" the height of the beam with a crack length $l = \beta h$. When the load on the cantilever beam, mentioned above, is prevented to move, the energy balance, eq.(7.7) becomes:

$$0 = E_e + E_c, \text{ or: } E_c = -E_e = -V\delta/2 \tag{7.10}$$

for the same crack length and now the energy of crack extension is equal to the decrease of elastic energy in the beam.

When the joint at load *V* becomes determining and just start to flow at δ_1 when splitting of the beam occurs, then eq.(7.7) becomes:

$$V\delta = (V\delta_1)/2 + V(\delta - \delta_1) + E_c \tag{7.11}$$

where again $V\delta_1/2$ is the increase of the elastic energy and $V(\delta - \delta_1)$ the plastic energy of the flow of the joint. From eq.(7.11) then follows:

$$E_c = V\delta_1 / 2 \tag{7.12}$$

the same as eq.(7.8), despite of the plastic deformation.

For connections, plastic deformation in the last case will not yet occur because it is coupled with crack extension. When the dowels of the joint are pressed into the wood, the crack opening increases and thus also crack extension. It can be seen in eq.(7.11), that when flow occurs, the total applied energy $V\delta$ is used for plastic deformation. This is a comparable situation as given by eq.(7.10), and the at the plastic flow coupled crack extension will cause a decrease of the elastic energy. eq.(7.11) thus for joints is:

$$\mathrm{V}\delta = (\mathrm{V}\delta_1 - \delta_2)/2 + V(\delta - \delta_1) + E_s \tag{7.13}$$

where $V\delta_2 / 2$ is the decrease of the elastic energy by the part of crack extension due to the plastic deformation. From eq.(7.13) now follows:

$$E_s = V(\delta_1 + \delta_2)/2 \tag{7.14}$$

and eq.(7.9) becomes:

$$V = \sqrt{\frac{2G_f bh}{\partial((u_1 + u_2)/V)/\partial\beta}} \tag{7.15}$$

From eq.(7.12) and (7.14) follows that $V_c\delta_{1c} = V(\delta_1 + \delta_2)$, where $V_c\delta_{1c}$ is the amount when the connection is as strong as the beam. Thus:

$$\frac{\delta_1 + \delta_2}{\delta_{1c}} = \frac{V_c}{V} = \frac{n_c V_n}{nV_n} = \frac{n_c}{n} \tag{7.16}$$

where V_n is the ultimate load of the dowel at flow and *n* the number of dowels.

Substitution of eq.(7.16) into eq.(7.15) gives:

$$V = \sqrt{\frac{2G_f bh}{\partial(u_{1c}/V)/\partial\beta} \cdot \frac{n}{n_c}} \tag{7.17}$$

what is equal to $\sqrt{n/n_c}$ times the strength according to eq.(7.9) for $u = u_{1c}$, thus $\sqrt{n/n_c}$ times the splitting strength of the beam as is applied in [1].

According to eq.(7.13), the theoretical lower bound of *V* according to eq.(7.17) occurs at $\delta_1 = \delta_2$, Thus when n/n_c = 1/2. In [1], the empirical value of 0.5 to 0.4 is mentioned according to the data giving:

$$V = \sqrt{\frac{2G_f bh}{\partial(u_{1c}/V)/\partial\beta}} \cdot \sqrt{0,45} = \sqrt{\frac{2G_f bh}{\partial(u_{1c}/V)/\partial\beta}} \cdot 0.67 \tag{7.18}$$

This requirement for "flow" of the joint at failure: $\sqrt{GG_f}$ = 0,67·18 = 12 $\mathrm{Nmm}^{-1.5}$ is included in the Eurocode (see Section 7.5).

The condition $\delta_1 = \delta_2$ means that there is sufficient elastic energy for total unloading and thus full crack extension with sufficient external work for plastic dissipation by the joints. According to eq.(7.13) is for that case:

$$E_c = V\delta_1 \tag{7.19}$$

7.3. Experimental Verification

The value of E_c of eq.(7.19) is 12 $\mathrm{Nmm}^{-1.5}$ as follows from the test data given in [1]. In [1], first test-results of 50 beams of [4] with one or two dowel connections are given of beams of 40x100 and 40x200 mm with $\alpha-$values between 0.1 and 0.7 and dowel diameters of 10 and 24 mm. In all cases $n \le 0.5 \cdot n_c$ and not splitting but flow of the connection is determining for failure reaching the in [1] theoretical explained high embedding strength by hardening as to be expected for the always sufficient high spreading possibility of one- (or two-) dowel joints. The same applies for the 1 and 2 dowel joints of the Karlsruhe investigation. Splitting then is not the cause of failure but the result of post-failure behaviour due to continued extension by the testing device.

Table 7.1 of [1] shows that for series B, splitting of the beam is determining. Whether there are 10, 15, 20 or 25 nails per shear plane, the strength is the same: $\sqrt{GG_c} = 16.7$ $\mathrm{Nmm}^{-1.5}$. This is confirmed by the too low value of the embedding strength of the nails f_c of series B. A more precise value of $\sqrt{GG_c}$ follows from the mean value of 17.1 $\mathrm{Nmm}^{-1.5}$ of series B2 to B4. Then the value for 10 nails of series B1 is a factor 15.5/17.1 = 0.9 lower.

Thus $\sqrt{n/n_c} = \sqrt{10/n_c} = 0.9$. Thus $n_c = 12$ for series B. This means that the number of 5 nails of series A is below $n_c/2 = 6$ and the measured apparent value of $\sqrt{GG_c}$ is the minimal value of $\sqrt{GG_c} \cdot \sqrt{0.5 n_c/n_c} = 17.1 \cdot \sqrt{0.5} = 12.1$ $\mathrm{Nmm}^{-1.5}$. The same value should have been measured for series C because the number of 3 nails also is below $n_c/2 = 6$. Measured is 11.7 $\mathrm{Nmm}^{-1.5}$. For the 53 beams of all the series G of [1] this is 12.0 $\mathrm{Nmm}^{-1.5}$. As mentioned a mean value of 12 is now the Eurocode requirement.

The value of $0.5 \cdot n_c$, depends on dimensioning of the joint and thus on amount of hardening by the spreading effect of embedding strength. Thin, long nails at larger distances

in thick wood members are less dangerous for splitting and show a high value of n_c. For series G, with b = 100 mm, $n_c/2$ is at least below 8 nails. For series V of [1] with dowels of 16 mm, $n_c = 8.6$. For design, n_c need not to be known. But dimensioning of the joint to meet also the requirement of $\sqrt{GG_c}$ = 12 $\mathrm{Nmm}^{-1.5}$, will lead to the number of nails of $n_c/2$. This dimensioning also determines the value of f_c. The value of f_c = 4.4 MPa of series A is lower than f_c = 6.2 MPa of series C, in proportion to the square root of the spreading lengths per nail as expected from theory [1].

Table 7.1. TU-Karlsruhe test data No.1: Joint with nails

Type	No	d	rows	Col	$a=\alpha h$	a_r	f_c	$\sqrt{GG_c}$	$\eta=L/h$	$F/b\alpha h$
Test	tests		m	N			[1]	eq.(7)		
		mm			mm	mm	MPa	$N/mm^{1.5}$		MPa
	beam: b.h=40.180 mm									
A1	8	3.8	5	1	28	76	3.7	13.9	2.37	7.37
A2	4	3.8	5	1	47	76	4.3	13.3	2.37	5.82
A3	3	3.8	5	1	66	76	4.2	11.3	2.37	4.52
A4	3	3.8	5	1	85	76	4.2	10.2	2.37	3.94
A5	3	3.8	5	1	104	76	5.5	11.7	2.37	4.54
	beam: b.h =40.180mm					**mean**	**4.4**	**12.1**		
B1	4	3.8	5	2	47	76	3.5	15.5	2.37	6.77
B2	3	3.8	5	3	66	76	3.8	17.9	2.37	7.15
B3	3	3.8	5	4	85	76	3.3	16.1	2.37	6.21
B4	3	3.8	5	5	104	76	3.6	17.2	2.37	6.69
	beam: b.h = 40.120 m					**mean**	**3.6**	**16.7**		
C1	3	3.8	2	1	28	76	6.8	15.3	2.18	8.51
C2	3	3.8	2	1	28	57	6.2	13.0	2.26	7.21
C3	3	3.8	2	1	28	38	5.6	10.9	2.34	6.07
C4	3	3.8	2	1	28	19	5.7	10.3	2.42	5.73
C5	3	3.8	1	1	28	0	6.9	11.2	2.50	6.21
C6	3	8	1	1	28	0	5.8	9.7	2.50	5.40
	beam: b.h=40.180 mm					**mean**	**6.2**	**11.7**		
L8	1	8	1	1	28	0	5.0	8.8	2.50	4.64

7.4. Design Equation of the Eurocode 5

As discussed in [1], the shear capacity is (for $h_e \leq 0.7\,h$)

$$\frac{V_u}{b\sqrt{h}} = 10.3\sqrt{\frac{\alpha}{(1-\alpha)}} = 10.3\sqrt{\frac{h_e}{(h-h_e)}}$$

where

$10.3 = (2/3)\sqrt{(GG_c / 0.6)}$ is the characteristic value.

This can be replaced by the tangent line through this curve at pointα = 0.5 giving:

$$\frac{V_u}{b\alpha\sqrt{h}} = 1.7\sqrt{GG_c} = 1.7 \cdot (2/3) \cdot 12 = 13.6 \ \text{Nmm}^{-1.5}.$$

7.5. References

[1] T.A.C.M. van der Put, A.J.M. Leijten, Evaluation of perpendicular to the grain failure of beams, caused by concentrated loads of joints. CIB-W18A/33-7-7, meeting 33, Delft, The Netherlands, August 2000.

[2] T.A.C.M. van der Put, Tension perpendicular to the grain at notches and joints. CIB-W18A-23-10-1, meeting 23, Lisbon, Portugal, Sept. 1990

[3] DWSF Technical note

[4] M. Ballerini: A set of tests on beams loaded perpendicular to the grain by dowel type of joints. CIB-W18/32-7-2. Graz. Austria.

CONCLUSION

- Because the failure criterion for "clear" wood and for macro-crack extension is the same, fracture mechanics of wood and comparable materials is determined by small-crack propagation towards the macro-crack tip. The influence of small-crack propagation is noticeable by the Weibull volume effect of the strength. There is no influence on macro-crack propagation of the geometry of notches and sharpness of the macro crack-tip in wood (against orthotropic theory). Thus orthotropic fracture mechanics is not determining. This also follows from the nearly same fracture toughness and energy release rate for wide and slit notches and the minor influence of rounding the notch (again against orthotropic theory). Determining thus is the influence of small cracks in the isotropic matrix for the total behaviour, having the same influence at the tip of wide as well as slit notches.
- The always applied singularity approach of fracture mechanics does not satisfy the limit analysis requirements for orthotropic materials and prevents the use of the right failure criterion at the crack boundary. Instead therefore, the complete solution of the Airy stress function, based on the flat elliptical crack, has to be applied.
- The empirical mixed I-II-mode fracture criterion is explained by the elliptical small-crack approach, providing the exact theoretical basis of this criterion. This criterion is the consequence of the ultimate uniaxial cohesive strength along the micro-crack boundary. The theory therefore also explains the relations between K_{Ic} and K_{IIc} in TL- and in RL-direction and the relations between the related fracture energies. This

leads to one overall apparent critical energy release rate which may be different for different structures but is independent of the stress combinations of the dissipated strain energy of fracture. Whether, for a square end-notch, work is done by only bending or by only shear deformation, failure is in mode I and not in mode II in the last case as predicted by the other models.

- The orthotropic approach, based on equilibrium of the homogenized reinforcement in wood gives incorrect results, because the matrix is not in equilibrium and does not satisfy the strength criterion. It therefore is necessary to start with equilibrium, compatibility and strength requirements of the isotropic matrix stresses providing a simple orthotropic-isotropic transformation of the Airy-stress function. for the total solution.
- Based on this approach is: $K_{Ic} = \sqrt{E_y G_{Ic}}$, $K_{IIc} = n_6 \sqrt{E_y G_{IIc}}$ and $G_{IIc} = 4G_{Ic}$ $G_f = 4G_{Ic}/(1+\sqrt{\gamma})^2 = G_{IIc}/(1+\sqrt{\gamma})^2$ with : $\gamma = 1/\left(1+\tau_{xy}^2/\sigma_y^2\right)$ and: $n_6 = \left(2+\nu_{21}+\nu_{12}\right)\cdot\left(G_{xy}/E_y\right)$
- The theoretical value of $G_{IIc} = 4G_{Ic}$ is verified by reported measurements where ratio 3.5 is found (R^2 = 0.64) instead of 4. This lower measured ratio is due to the applied too high value of G_{Ic} which should be corrected to be equal to the energy release rate.
- It is shown, that the models applied to wood, (as necessary replacement of the infinite fracture stresses of the singularity approach), as e.g. the Dugdale model, fictitious crack model and crack growth models are incorrect and have to be replaced by the general theory.
- A derivation of the softening curve is given based on small-crack extensions. The softening curve follows at the start the stable part of the Griffith locus. This means that every point of the softening curve gives the Griffith strength. This curve depends on only one parameter, the maximal critical Griffith stress σ_c and therefore depends on the critical crack density. This applies until half way of unloading. The fracture energy is down to this point equal to the critical energy release rate. After that, the strength of the fracture plane of the test specimen becomes determining due to a crack joining mechanism, changing the crack density and intact area of the fracture plane and therefore causing a decrease of σ_c and an apparent decrease of the fracture energy. The strength at every point of the softening curve is fully determined by the strength of the intact area of the fracture plane. Softening thus is a matter of elastic unloading of the specimen outside the fracture zone and softening thus is not a material property.
- The fracture energy for mode I is stated in literature to be equal to the area under the softening curve divided through the crack length. This is not right. It is half this area when the fracture plane is not limiting. This is applied and accepted for mode II in wood.
- It also is stated that the area of a loading cycle at softening, divided by the area of the crack increment, is equal to the fracture energy. This also is not right. It is shown that

this energy is proportional to the apparent activation energy of all processes in the whole test specimen.

- A revision is necessary of all published mode I data of the fracture energy, based on the area of the softening curve, because of the dissimilar behaviour of post fracture behaviour giving no right prediction of the fracture energy. Therefore this area method should not be used anymore. A right simple description follows from the derived apparent energy release rate adapted to the measured strength data.
- The theory shows that the Eurocode design rules for beams with rectangular end notches or joints should be corrected to the right real compliance difference and the right measured uniaxial stiffness.
- The verification of the derived theory by measurements shows the excellent agreement. The method provides an exact solution and is shown to be generally applicable also for joints and provides as simple design equations as wanted.

9. APPENDIX: WEIBULL SIZE EFFECT IN FRACTURE MECHANICS OF WIDE ANGLE NOTCHED TIMBER BEAMS

Because the Weibull size effect is normally not a fracture mechanics subject, this influence is discussed in a separate appendix to the main theory of this chapter.

9.1. Summary

A new explanation is given of the strength of wide angled notched timber beams by accounting for a Weibull type size effect in fracture mechanics. The strength of wood is described by the probability of critical initial small crack lengths. This effect is opposed by toughening by the probability of having a less critical crack tip curvature. The toughening effect dominates at the different wide angle notched beams showing different high stressed areas by the different angles and thus different influences of the volume effect. This is shown to explain the other power of the depth in Eq.(9.18) and (9.19) than the sharp notch value of 0.5 of Eq.(9.17). It further is shown to explain why for very small dimensions, also for sharp notches, the volume effect applies. The explanation by the Weibull effect implicates that the strength depends on small crack extension, in the neighbourhood of the macro crack tip. This initial crack population can be different for full scale members indicating that correction of the applied data is necessary and that additional toughness tests have to be done on full scale (or semi full scale) test specimens.

9.2. Introduction

Fracture mechanics of wood is normally restricted to fracture along the grain. It is e.g. not possible to have shear crack propagation across the grain. Also the mixed mode crack follows the weak material axes and only may periodically jump to the next growth layer at a weak spot. Thus the direction of the collinear crack propagation is known and is not e.g. dependent

on a local critical value of a strain energy density. As shown in [1], the singularity approach gives no right results in this case and the analysis has to be based on linear elastic flat elliptic crack extension by the maximal stress at the elastic-plastic boundary around the small crack. This response at randomized stress raisers near weak spots is indicated by the volume effect of the strength. There also is no clear influence on macro-crack propagation of the crack geometry and notch form and sharpness of the macro crack tip, showing orthotropic fracture mechanics to be not decisive. This also is indicated by the not orthotropic, but isotropic relation between mode I stress intensity and strain energy release rate of wood. The determining small crack behaviour also follows from the failure criterion of common un-notched wood being of the same form as the theoretical explained fracture mechanics criterion for notched wood.

Wood should be regarded as a reinforced material. The commonly applied orthotropic Airy stress function is based on spread out of the reinforcement to act as a continuum, satisfying the equilibrium, compatibility and strength conditions. This only is possible by interaction through the matrix and the solution by the orthotropic plane equilibrium methodappears to be not right because thedetermining equilibrium conditions and strength criterion of the matrix then are not satisfied. It thus is necessary to solve the Airy stress function for the stresses in the isotropic matrix and this appears to give the right solution providing the theoretical derivation [1] of the Wu-mixed mode I - II fracture criterion. As a result, the right fracture energies and theoretical relations between mode I and II stress intensities and energy release rates then are obtained. This also applies for the relations between the mode I critical stress intensities of the different main material planes. For wood the matrix thus is determining for initial failure and not the reinforcement.Also the failure criterion of unnotched wood shows no coupling term between the reinforcements in the main directions confirming the orthotropic strength schematization to be not determining. The determining small crack dimension follows from the Weibull size effect. The here treated strength of wide angle notched beams is an example of a determining size effect in fracture mechanics.

The strength analysis of [2] of wide angle notched beams, given in Figure9.1, was based on the orthotropic Airy stress function. However, despite of the dominant mode I loading, none of the solutions of this function are close enough to the measurements to be a real solution. The reason of this is the absence of the Weibull size effect in the equations as will be shown in this article. The in [2] chosen solutions of the biharmonic Airy stress function are:

$r_1^{\pm n}\cos(n\theta_1)$, $r_1^{\pm n}\sin(n\theta_1)$, $r_2^{\pm n}\cos(n\theta_2)$, $r_2^{\pm n}\cos(n\theta_2)$ resulting in:

$$\{\sigma_r,\sigma_\theta,\sigma_{r\theta}\}=\frac{K_A}{(2\pi r)^n}\{f_1(n\theta),f_2(n\theta),f_3(n\theta)\} \tag{9.1}$$

where K_A is the stress intensity factor and "r" the distance from the notch root. In the direction of crack extension, along the grain ($\theta=0$), the tensile strength perpendicular to the grain σ_θ is determining for fracture. The boundary conditions for the different notch angles

a/g provide different values of the power "*n*"and thus different slopes of the lines in Figure 9.2. However, it is theoretically not possible that these lines intersect trough one point, as is measured, because the different boundary conditions by the different notch angles cannot be satisfied at the same time and the chosen mathematical solution of [2] thus have to be rejected. The fact that these lines cross one point, at the elementary volume, indicates the existence of a volume effect of the strength. This has to be introduced in the fracture mechanics calculation what simply can be based on the energy method as discussed in section 9.4.

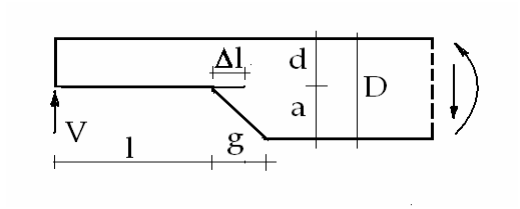

Figure9.1. Wide angle notched beam element.

In section 9.3, the derivation of the size effect is given to show the analogous derivation of the toughening size effect in section 9.4.

9.3. Size Effect

Due to the initial small crack distribution, clear wood shows a brittle like failure for tension and shear.According to the Weibull model, the probability of rupture, due to propagation of the biggest crack in an elementary volume V_0 is equal to $1-P_0(\sigma)$, when P_0 is the probability of survival. For a volume *V* containing $N = V / V_0$ elementary volumes the failure probability is $1-P_s = (1-P_0)(1-P_0)(1-P_0)\cdots = (1-P_0)^N$. Thus $\ln(1-P_s) = N\ln(1-P_0) \approx -NP_0$ because $P_0 << 1$. Thus the probability of survival of a specimen with volume *V*, loaded by a constant tensile stress σ, as in the standard tensile test, is given by:

$$P_s(V) = \exp(-NP_0) = \exp\left(-\frac{V}{V_0}\left(\frac{\sigma}{\sigma_0}\right)^k\right) \tag{9.2}$$

where $P_0(\sigma) = (\sigma/\sigma_0)^k$ is chosen, because the power law of σ may represent any function of σ around a chosen stress value as e.g. the mean failure stress (see Section 9.5 for the proof). For a stress distribution, Eq.(9.2) becomes:

$$P_s(V) = \exp\left(-\int_V \left(\frac{\sigma(x,y,z)}{\sigma_0} \right)^k dx \cdot dy \cdot dz / V_0 \right) \tag{9.3}$$

This specimen has an equal probability of survival as the standard test specimen Eq.(9.2) when the exponents are equal thus when:

$$\int_V \left(\frac{\sigma(x,y,z)}{\sigma_0} \right)^k dV = \left(\frac{\sigma_s}{\sigma_0} \right)^k V_s \tag{9.4}$$

For a constant stress $\sigma(x,y,z) = \sigma$, the specimen strength thus will decrease with its volume *V* according to:

$$\sigma = \sigma_s \cdot \left(\frac{V_s}{V} \right)^{1/k} \tag{9.5}$$

where σ_s is the mean strength of the specimen with volume V_s. The power *k* depends on the coefficient of variation s/σ according to:

$$\left(\frac{\mathrm{s}}{\sigma} \right)^2 = \frac{\Gamma(1+2/\mathrm{k})}{\Gamma^2(1+1/\mathrm{k})} - 1 \tag{9.6}$$

From the row-expansion of the Gamma-functions it can be seen that:

$$k \cdot \frac{s}{\sigma} = f\left(\frac{s}{\sigma} \right) \approx 1.2 \tag{9.7}$$

where f(s/σ) is normally a little varying function. Thus: $1/k = s/(1.2 \cdot \sigma)$

For a stress distribution, Eq.(9.4) becomes:

$$\int \left(\frac{\sigma_m}{\sigma_0} \right)^k \left(\frac{\sigma(x,y,z)}{\sigma_m} \right)^k dxdydz = \left(\frac{\sigma_m}{\sigma_0} \right)^k V_{ch} = \left(\frac{\sigma_s}{\sigma_0} \right)^k V_s \tag{9.8}$$

where σ_m is the determining maximal stress in volume *V* and $V_{ch} = \int (\sigma/\sigma_m)^k dV$, a characteristic volume. Eq.(9.8) thus becomes:

$$\sigma_m = \sigma_s \left(\frac{V_s}{V_{ch}} \right)^{1/k} = \sigma_s \left(\frac{V_s}{V_{ch}} \right)^{s/1.2\sigma} \tag{9.9}$$

This applies for the strength of common unnotched specimens.
This strength also is determined by fracture mechanics. The tensile strength is e.g.:

$$f_t = \frac{K_{Ic}}{\sqrt{\pi c}} \quad \text{or} \quad f_t = f_{t,s}\sqrt{\frac{c_s}{c}}\,. \tag{9.10}$$

where K_{Ic} is the stress intensity factor.
Substitution of the strength according to Eq.(9.5) (or Eq.(9.9)) leads to:

$$f_t = f_{t,s}\sqrt{\frac{c_s}{c}} = f_{t,s,V}\left(\frac{c_s}{c}\right)^{0.5}\left(\frac{V_s}{V}\right)^{1/k} \tag{9.11}$$

This equation gives the probability of a critical Griffith crack length *c* leading to fracture. Also in this case, a crack toughening mechanism is thinkable,discussed in section 9.4, leading to the opposite volume effect with a negative value of the exponent 1/*k*. This can not be distinguished and the resultant value of 1/*k* then is given by Eq.(9.11). Because for every type of wood material the value of *c* is specific, determining the specimen strength, Eq.(9.9), as shortcut of Eq.(9.11), is applied in practice.

The fracture mechanics derivation for wood can be based on the elastic full "plastic" approximation of flow and microcracking at the crack tip. Thus the crack dimensions are replaced by the elastic-plastic boundary around the crack and linear elastic fracture mechanics is applicable outside this boundary. According to [3], the stress intensity factor of Eq.(9.10) is: $K_{Ic} = \sigma_t\sqrt{\pi r/2}$ where σ_t is the equivalent cohesion strength at the crack tip boundary and r is the radius of the elastic-plastic boundary of the crack tip zone. A constant stress intensity factor K_{Ic} means that $\sigma_t\sqrt{r}$ is constant and only the crack length *c* is a variable as for brittle fracture. Toughening means an increase of the plastic zone, thus of *r* of the small cracks, within the characteristic volume. This influence is visible at the different wide angle notches as discussed in section 9.4.

Because fracture across the grain is tough and the lengths of applied beams don't vary much, the size effect of the length dimension is small and the volume effect for bending is replaced by a height effect of the beam only. It is postulated that this absence of a width effect is explained by the constant widths of $2b'$ of2 planes of weakness adjacent to the sides of the beam due to cutting at manufacturing. Then: $\left(V_s/V_{ch}\right)^{1/k} = \left(2b'h_s l/2b'hl\right)^{1/k} = \left(h_s/h\right)^{1/k}$, becomes the height factor of the Codes. This width effect is applied in section 9.4.

9.4. Size Effect of Wide Notched Beams

The analysis of the strength of the notched beams can be based on the energy method where the critical fracture energy is found from the difference of the work done by the constant force due to its displacement by a small crack extension minus the increase of the strain energy due to this displacement. According to this approach of [3], the bending stress σ_m at the end of the notched beam at $l = \beta D$ in Figure 9.1 is:

$$\sigma_m = \frac{6V_f \beta D}{b(\alpha D)^2} \approx \frac{\sqrt{6EG_c / D}}{\sqrt{\left(\alpha - \alpha^4\right)}} \tag{9.12}$$

when the notch is not close to the support. In [2] is chosen: α = *d/D* = 0.5, what means that *d* = *a*.Further the length is *l* = 2*D* when *g/a* = 0 and 2, while *l* = 4D for *g/a* = 4in Figure 9.1.*E* is the modulus of elasticity and G_c the critical energy release rate, given in [3]. Eq.(9.12) applies for the rectangular notch (*g* = 0). For wide notch angles a more complicated expression applies because of the changing stiffness over length Δl of the crack extension. However, for given dimensions and loading, the basic form of the equation is the same as Eq.(9.12), thus:

$$\sigma_m = B\sqrt{EG_c / D} \tag{9.13}$$

where *B* is a constant depending on dimensions and notch angle. According to [3] is, as mentioned, $\sqrt{EG_c} \triangleq K_c \triangleq \sigma_t \sqrt{r}$, where σ_t is the equivalent cohesion strength and the crack tip radius r is the only parameter of the notch strength. The volume effect depending on the stress follows from section 9.3 and the analysis thus can be based on the flow stress and the characteristic volume around the notch tip, For the probability of a critical value of *r*, of the small initial cracks within the high stressed characteristic volume around the notch tip, the probabilistic reasoning of section 9.3 can be repeated as follows. The probability of having a critical flaw curvature $1/r$ in an elementary volume V_0 is equal to $1 - P_0(1/r)$, when P_0 is the survival probability. For a volume *V* containing $N = V/V_0$ elementary volumes the survival probability is in the same way:

$$P_s(V) = \exp\left(-NP_0\right) = \exp\left(-\frac{V}{V_0}\left(\frac{r}{r_0}\right)^{-k}\right) \tag{9.14}$$

where $P_0\left(1/r\right) = \left(r_0 / r\right)^k$, because the power law may represent any function in 1/*r*. At "flow", this probability is not a function of σ, but of the flow strain, given by critical *r*

Equal exponents for the same probability of failure in two cases now lead to:

$$r = r_s \left(V / V_s \right)^{1/k} \tag{9.15}$$

and Eq.(9.13) becomes:

$$\sigma_m \approx \frac{B'\sigma_t \sqrt{r_s}}{\sqrt{D}} \cdot \left(\frac{V}{V_s} \right)^{1/2k} \quad \text{or:} \quad \sigma_m = \sigma_{m0} \left(\frac{D}{D_0} \right)^{-0.5} \left(\frac{V}{V_0} \right)^{1/2k} \tag{9.16}$$

For the notch angle of 90°, (g = 0 in Figure 9.1), or smaller angles, the high stressed elastic region around the crack tip is, as the fracture process zone itself, independent of the beam dimensions. Thus in characteristic dimensions $V = b'l'h' = V_0$ and Eq.(9.16) becomes:

$$\sigma_m = \sigma_{m0} \left(\frac{D}{D_0} \right)^{-0.5} . \tag{9.17}$$

independent of a volume effect. For the widest notch angle of 166° (g/a = 4), there is a small stress gradient over a large area and V is proportional to the beam dimensions. Thus: V (:) $b \cdot d \cdot l = \gamma D \cdot \delta D \cdot \beta D = \gamma \cdot \beta \cdot \delta \, D^3$ and: $V/V_0 = (\gamma\delta\beta \, D^3 / \gamma\delta\beta \, D_0^3) = \left(D / D_0 \right)^3$. Thus is, with $1/k$ = 0.18:

$$\sigma_m = \sigma_{m0} \left(\frac{D}{D_0} \right)^{-0.5+3/(2k)} = \sigma_{m0} \left(\frac{D}{D_0} \right)^{-0.23} \tag{9.18}$$

For the angle of 153.40°, (g/a = 2), the high stressed region dimensions becomes proportional to the dimensions b and D and:

$V/V_0 = (bdl)/(b_0 d_0 l) = (\gamma\delta D^2 / \gamma\delta D_0^2) = (D^2 / D_0^2)$ and with$1/k$ = 0.18 is:

$$\sigma_m = \sigma_{m0} \left(\frac{D}{D_0} \right)^{-0.5+2/(2k)} = \sigma_{m0} \left(\frac{D}{D_0} \right)^{-0.32} \tag{9.19}$$

It follows from Figure9.2, that the values of exponents of – 0.5, - 0.32, and -0.23 are the same as measured. The coefficient of variation of the tests must have been: 1.2·0.18 = 0.22, as common for wood. According to the incomplete solution of [2], discussed in the Introduction, these values of the exponents were respectively - 0.437, - 0.363 and - 0.327, thus too far away from the measured values.

The explanation of no volume effect of sharp notches due to the invariant characteristic volume,independent of the beam dimensions, explains also why for very small beams, also for sharp notches, there is a volume effect because then the beam dimensions are restrictive for the characteristic volume. As shown above, the exponent may change from – 0.5 to -0.23

with decrease of the beam dimensions. This is measured and e.g. discussed at pg. 85 of [4] and it now is shown that toughening (and not nonlinear behaviour) is the explanation of this volume effect.

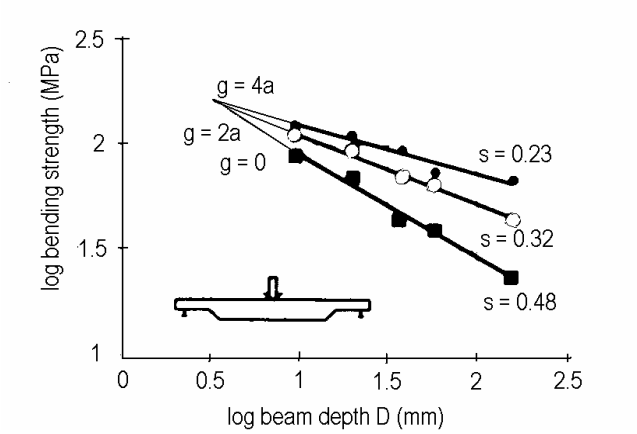

Figure 9.2. Measured bending strengths for different sizes and notch angles.

The lines in Figure 9.2 intersect at the elementary Weibull volume wherefore the depth dimension is $10^{0.6} = 4$ mm with a material bending strength of 147 MPa.

9.5. Derivation of the Power Law Applied in Section 9.3

Any function f(x) always can be written in a reduced variable x / x_0.

$$f(x) = f_1(x / x_0)$$

and can be given in the power of a function:

$$f(x) = f_1(x / x_0) = \left[\left\{ f_1\left(x / x_0\right) \right\}^{1/n} \right]^n \quad \text{and expanded into the row:}$$

$$f(x) = f(x_0) + \frac{x - x_0}{1!} \cdot f'(x_0) + \frac{(x - x_0)^2}{2!} \cdot f''(x_0) + \ldots\ldots \text{ giving:}$$

$$f(x) = \left[\left\{ f_1(1) \right\}^{1/n} + \frac{x - x_0}{x_0} \frac{1}{n} \left\{ f_1(1) \right\}^{1/n-1} \cdot f_1'(1) + \ldots\ldots \right]^n = f_1(1) \cdot \left(\frac{x}{x_0} \right)^n$$

when: $\left(f_1(1) \right)^{1/n} = \left(f_1(1) \right)^{1/n-1} \cdot f_1'(1) / n$ or: $n = f_1'(1) / f_1(1)$

where: $f_1'(1) = \partial f_1(x/x_0)/\partial(x/x_0)$ for $x = x_0$ and $f_1(1) = f(x_0)$

Thus: $f(x) = f(x_0)\cdot\left(\frac{x}{x_0}\right)^n$ with $n = \frac{f_1'(1)}{f_1(1)} = \frac{f'(x_0)}{f(x_0)}$

This derivation of the power law, using only the first 2 expanded terms applies in a limited range of *x* around x_0. This is not restrictive for strength problems. and one reference value x_0 is sufficient.

9.6. Conclusions Regarding the Size Effect

- A explanation is given of the strength of wide angled notched beams of [2] by introducing the Weibull type size effectin fracture mechanics based on the critical curvature of the initial small cracks near the high stressed notch tip zone.
- For sharp notch angles, up to 90°, there is no volume effect due to the constant volume of the characteristic volume, containing the fracture process zone. For wider notch angles, the peak stresses and stress gradients become lower and are divided over a larger region and influenced by the dimensions and thus a volume effect correction applies.
- The intersect of the three lines in Figure9.2, with different values of "*n*" of Eq.(9.1), due to different boundary conditions by the different notch angles, can not be explainedby the boundary value analysis. This intersect only can be explained to be due to the volume effect of the strength indicating failure by small crack extension within the high stressed region at the notch tip.
- Using the Energy approach and the volume effect correction according to Eq.(9.16), the measured values of the powers of the depths (or the slopes of the lines of Figure9.2) are precisely explained.

9.7. References

[1] T.A.C.M. van der Put, A new fracture mechanics theory of orthotropic materials like wood, *Eng. Fract. Mech*. 74, (2007), 771-781.

[2] R.H. Leicester, Design specifications for notched beams in AS 1720, CIB-W18/38-6-1, meeting 38, Karlsruhe, Germany, August 2005.

[3] T.A.C.M. van der Put, Modified energy approach for fracture of notched beams, COST 505 workshop on fract. mech. Bordeaux, April 1992.

[4] Smith, E. Landis, M. Gong, *Fracture and Fatigue in Wood*, J. Wiley & Sns.